JPRS L/9274

27 August 1980

USSR Report

EARTH SCIENCES

(FOUO 7/80)

FBIS FOREIGN BROADCAST INFORMATION SERVICE

APPROVED FOR RELEASE: 2007/02/08: CIA-RDP82-00850R000300020046-6

NOTE

JPRS publications contain information primarily from foreign newspapers, periodicals and books, but also from news agency transmissions and broadcasts. Materials from foreign-language sources are translated; those from English-language sources are transcribed or reprinted, with the original phrasing and other characteristics retained.

Headlines, editorial reports, and material enclosed in brackets [] are supplied by JPRS. Processing indicators such as [Text] or [Excerpt] in the first line of each item, or following the last line of a brief, indicate how the original information was processed. Where no processing indicator is given, the information was summarized or extracted.

Unfamiliar names rendered phonetically or transliterated are enclosed in parentheses. Words or names preceded by a question mark and enclosed in parentheses were not clear in the original but have been supplied as appropriate in context. Other unattributed parenthetical notes within the body of an item originate with the source. Times within items are as given by source.

The contents of this publication in no way represent the policies, views or attitudes of the U.S. Government.

For further information on report content call (703) 351-2938 (economic); 3468 (political, sociological, military); 2726 (life sciences); 2725 (physical sciences).

APPROVED FOR RELEASE: 2007/02/08: CIA-RDP82-00850R000300020046-6

JPRS L/9274

27 August 1980

USSR REPORT

EARTH SCIENCES

(FOUO 7/80)

CONTENTS

OCEANOGRAPHY

UDC 551.466.326

MEASUREMENT OF FREQUENCY AND ANGLE SPECTRA OF WIND WAVES USING A WAVE RECORDER ARRAY

Sevastopol' MORSKIYE GIDROFIZICHESKIYE ISSLEDOVANIYA in Russian No 3, 1979 pp 75-86

[Article by Yu. P. Solov'yev and V. V. Yefimov]

Abstract: The article discusses methods for evaluating the spectrum of frequencies and wave numbers using the results of synchronous measurements of the sea surface rise at several points. The authors compare the traditional method and the maximum probability method for evaluations of stipulated models of the angle spectrum. Experimental evaluations of the frequency-angle spectra of wind waves in the coastal zone of the open sea are given for the case of a stable wind field. Their difference from known approximations of the angular distribution functions for the energy of wind waves is considered.

[Text] Interest in study of the spatial characteristics of the random field of wind waves is associated both with the practical purposes of a forecast and with the necessity for a detailed investigation of the properties of the wind waves themselves. The spectrum of frequencies and wave numbers $F(\vec{k}, \omega)$ completely describes the distribution of the energy of wind waves at temporal and spatial scales. In a linear approximation $F(\vec{k}, \omega)$ is reduced to a frequency-angle spectrum determining the distribution of the energy of wave components by directions. At the present time there is no theory which predicts the form or width of the angle spectrum. It is clear from general considerations that the angle spectrum governs the structure of the air flow over the wave-covered sea surface, for example, the stability of wind direction and its velocity, the duration of its effect, fetch and other factors. The precise form of this dependence is unknown.

The few results of measurements of the spatial characteristics of the field of wind waves obtained using different methods [1, 7-9] have made it possible to draw some qualitative conclusions concerning the behavior of the

angle spectra. However, the inadequate resolution of the method and the great variability of the angle spectra in dependence on hydrometeorological conditions do not afford any possibility for an unambiguous determination of the functional form of the angle spectra.

Recently new methods have been developed and put in use in oceanography for the evaluation of $F(\vec{k}, \omega)$ which are more effective in the study of wave processes in comparison with the traditional methods. One of these is the maximum probability method (MPM) [2, 10, 11]. Evaluations of the maximum probability of $F(\vec{k}, \omega)$ on the basis of measurements with an array of sensors have better resolution with respect to directions and wave numbers in comparison with the Barber method [12].

In this study we present the results of computation of the angle spectra of wind waves obtained from synchronous measurements of the sea surface rise at several points and give a comparison of MPM evaluations and the Barber method.

Methods for Evaluating the Angle Spectra

We will represent the surface rise $\eta(\vec{x}, t)$ in the form of a Fourier-Stieltjes integral

$$\eta(\vec{x}, t) = \iint_{\vec{k}\,\omega} a(\vec{k}, \omega) \cdot \exp\left[i(\vec{k}\cdot\vec{x} - \omega t)\right] d\vec{k}\, d\omega, \tag{1}$$

where $\vec{x}$ is the horizontal position vector; t is time; $\vec{k}$ is the wave number vector; ω is cyclic frequency.

Then the spectrum of frequencies and wave numbers on the assumption of uniformity and stationarity of the wave field can be determined as

$$F(\vec{k}, \omega) = \frac{1}{(2\pi)^3} \iint B(\vec{r}, \tau) \exp\left[-i(\vec{k}\vec{r} - \omega\tau)\right] d\vec{r}\, d\tau, \tag{2}$$

where $B(\vec{r}, \tau) = \langle \eta(\vec{x}, t) \cdot \eta(\vec{x} + \vec{r}, t + \tau) \rangle$ is a spatial-temporal intercovariation function. From the definition of (2) it follows that

$$F(\vec{k}, \omega) = F(-\vec{k}, -\omega), \quad F(\vec{k}, \omega) \neq F(-\vec{k}, \omega). \tag{3}$$

According to (3), the spectrum $F(\vec{k}, \omega)$ for $\omega > 0$ unambiguously determines the direction of propagation of the wave components. Integrating $F(\vec{k}, \omega)$ for $\vec{k}$, it is possible to obtain the frequency spectrum

$$S(\omega) = \int_{\vec{k}} F(\vec{k}, \omega)\, d\vec{k} \tag{4}$$

and find the correlation between $F(\vec{k}, \omega)$ in rectangular (k_x, k_y) and polar (k, θ) coordinates

$$\kappa F(k_x, k_y, \omega) = \Phi(\kappa, \theta, \omega), \tag{5}$$

where θ is the angle between the x axis and the direction of the $\vec{k}$ vector. In a linear approximation (in the case of satisfaction of the dispersion expression $\omega^2 = gk$ for a deep sea) the spectrum $F(\vec{k}, \omega)$ is different from zero only in a circle with the radius $k = \omega^2/g$ and the spatial spectrum is reduced to a frequency-angle spectrum

$$\chi(\omega, \theta) = \int_0^\infty \Phi(\kappa, \theta, \omega)\, d\kappa = \int_0^\infty \psi(\kappa, \theta) \cdot \delta\left[\omega - \omega(\kappa)\right] d\kappa = \tag{6}$$

$$= \int_0^\infty \psi(\kappa, \theta) \frac{d\kappa}{d\omega} \delta\left[\kappa - \kappa(\omega)\right] d\kappa = \frac{2\omega}{g} \psi(\kappa, \theta)\Big|_{\kappa = \frac{\omega^2}{g}} = \frac{2\omega^3}{g^2} \psi(\vec{\kappa})\Big|_{\kappa = \frac{\omega^2}{g}}.$$

For evaluating $\hat{F}(\vec{k}, \omega)$ of the true spectrum $F(\vec{k}, \omega)$ we use data from synchronous measurements of $\eta(\vec{x}, t)$ at N points with the coordinates $\vec{r}_i$. Using the Barber method [12], the mathematical expectation $\hat{F}(\vec{k}, \omega)$ is determined by the expression

$$\langle \hat{F}(\vec{\kappa}, \omega) \rangle = \int_{\vec{\kappa}} \int_{\omega'} F(\vec{\kappa}', \omega') \cdot W(\vec{\kappa}, \vec{\kappa}') \cdot W(\omega, \omega')\, d\vec{\kappa}'\, d\omega', \tag{7}$$

where

$$W(\vec{\kappa}, \vec{\kappa}') = \sum_{i=1}^{N} \sum_{j=1}^{N} B_{ij} \exp\left[-i(\vec{\kappa} - \vec{\kappa}')\vec{r}_{ij}\right] = \sum_{i=1}^{N} \sum_{j=1}^{N} B_{ij} \cos(\vec{\kappa} - \vec{\kappa}')\vec{r}_{ij} - \tag{8}$$

the wave number spectral window; $W(\omega, \omega')$ is the frequency spectral window; $\vec{r}_{ij} = \vec{r}_j - \vec{r}_i$; B_{ij} are weighting factors; $B_{ij} = 1$ when $i \neq j$ and $B_{ij} = 1/N$ when $i = j$. On a practical basis the $F(\vec{k}, \omega)$ value is computed as

$$\hat{F}(\vec{\kappa}, \omega) = \sum_{i=1}^{N} \sum_{j=1}^{N} B_{ij} \left[q_{ij}(\omega)\right] \exp(-i\vec{k}\vec{r}_{ij}), \tag{9}$$

where $\left[q_{ij}(\omega)\right]$ is a spectral matrix whose diagonal elements are the values of the autospectra and when $i \neq j$ $q_{ij}(\omega) = P_{ij}(\omega) - iQ_{ij}(\omega)$, where $P_{ij}(\omega)$ are cospectra and $Q_{ij}(\omega)$ are quadrature spectra, computed for each pair of records at the points $\vec{r}_i$ and $\vec{r}_j$.

It can be seen from expression (8) that resolution with respect to $\vec{k}$ is entirely determined by the geometry of the array of wave recorders. In actuality (8) is an evaluation of a plane monochromatic wave of a unit amplitude with the wave number $\vec{k}$. As will be demonstrated below, waves whose lengths are comparable to the dimensions of the array are resolved best. The minimum size of the array determines k_{max}, which is an analogue of the Nyquist

frequency in the space of wave numbers. With an increase in wavelength the resolution worsens. In order to obtain the true $F(\vec{k},\omega)$ value it is necessary to carry out renormalization of the evaluation (9) with (4) taken into account.

The maximum probability method was developed and used for the first time in seismology for discriminating a quasidetermined signal against a noise background [10]. The use of the maximum probability method in oceanology also gave good results [2, 3, 11]. The MPM evaluation is computed using the expression

$$\hat{F}(\vec{k},\omega)=\left\{\sum_{i=1}^{n}\sum_{j=1}^{n}\left[q_{ij}(\omega)\right]^{-1}\exp\left(-i\vec{k}\vec{r}_{ij}\right)\right\}^{-1}, \qquad (10)$$

where $[q_{ij}(\omega)]^{-1}$ is a matrix which is the inverse of the spectral matrix in (9). A distinguishing characteristic of the MPM as an adaptive method is a dependence of the form of the spectral window of wave numbers on the parameters of the measured process. The geometry of the array, as in the Barber method, exerts an influence on such characteristics of the evaluation $F(\vec{k},\omega)$ as the maximum and minimum resolvable scales of the measured process and the selectivity of resolution with respect to directions. However, the principle for computing the MPM evaluation is based on the discrimination of a useful signal against a noise background and the method gives good results when the signal-to-noise ratio is small. The reason for the appearance of noise can be a whole series of factors: inaccuracy in the calibration of the wave recorders, discreteness of reading of amplitude data, selective variability of evaluations of the cross-spectra and the very nature of the measured process. The intensity of the noise arising as a result of the errors in measurement and processing can be decreased or at least taken into account. For example, in order to eliminate inaccuracies in the calibration of the wave recorders the evaluations $P_{ij}(\omega)$ and $Q_{ij}(\omega)$ are usually normalized to the values of the autospectra $S_i(\omega)$ and $S_j(\omega)$. The selective variability of evaluations of the cross spectra can be decreased by increasing the length of the initial records. In [11] the authors discussed the possibility of using the MPM for evaluating $F(\vec{k},\omega)$ of the random field of wind waves, characterized by a continuous distribution of energy by directions, and it was shown that in the case of a broad angle spectrum the method is ineffective. This conclusion can be illustrated by the following simple reasoning. The evaluations of the normalized $R_{ij}(\omega)$ and $Q_{ij}(\omega)$ values, entering into (10), can be represented in the form

$$\frac{P_{ij}(\omega)}{\left[S_i(\omega)\cdot S_j(\omega)\right]^{\frac{1}{2}}}=R_{ij}(\omega)\cdot\cos\varphi_{ij}(\omega),$$
$$\frac{Q_{ij}(\omega)}{\left[S_i(\omega)\cdot S_j(\omega)\right]^{\frac{1}{2}}}=-R_{ij}(\omega)\cdot\sin\varphi_{ij}(\omega), \qquad (11)$$

where $R_{ij}(\omega)$ is the coherence function; $\varphi_{ij}(\omega)$ is the phase spectrum. The theoretical value $R_{ij}(\omega)$, which is equal to 1 for plane waves, is dependent on the width of the angle spectrum and decreases with its broadening

[4]. This effect is manifested most strongly with bases $\vec{r}_{ij}$ perpendicular to the direction of wave propagation and is dependent on the ratio of wave length to $|r_{ij}|$. A decrease of $R_{ij}(\omega)$ is equivalent to the manifestation of additional noise associated with the character of the wave field and leads to a deterioration of MPM evaluations.

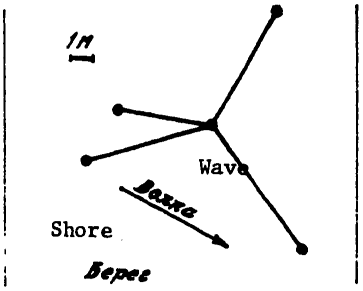

Fig. 1. Diagram of layout of wave recorders.

For evaluations of distortion of the true spectrum $F(\vec{k},\omega)$ introduced by the measurement and processing methods, we used the modeling method. The spectrum of frequencies and wave numbers was stipulated in the form

$$\frac{\Phi(\kappa,\theta,\omega)}{S(\omega)}=\begin{cases} A\cos^{n}\theta\cdot\delta(k-k_0), & |\theta|\leqslant\frac{\pi}{2}, \\ 0, & |\theta|>\frac{\pi}{2}, \end{cases} \tag{12}$$

where

$$A=\left[\int_{-\frac{\pi}{2}}^{\frac{\pi}{2}}\cos^{n}\theta\,d\theta\right]^{-1}.$$

The values of the elements of the spectral matrix for different n and k_0 values were computed for an array of wave recorders (Fig. 1). The selected computation accuracy was $\sim 10^{-3}$, which corresponds to the level of the spectrum of the noise of evaluations of real cross-spectra. The results are shown in Fig. 2, where for several n and k_0 values we have given the initial angle spectra (12), their evaluations by the maximum probability method and by the Barber method. Accordingly, MPM evaluations of the angular distributions of the form $\cos^{12}\theta$ are narrower and $\cos^{8}\theta$ and $\cos^{4}\theta$ are virtually undistorted. The distortions of the evaluation, associated with the appearance of spurious peaks, are observed only for high k_0 values. Evaluations by the Barber method, on the other hand, differ greatly from the initial spectra with narrow distributions and small k_0. With an increase in k the evaluations are improved and even exceed the MPM evaluation with $k_0 = 0.64\ m^{-1}$.

We note that the MPM evaluation is a biased $F(\vec{k},\omega)$ evaluation, but this shortcoming can be eliminated by normalization to the maximum value. The confidence intervals in evaluation by the MPM are found from the χ^2 distribution with the number of degrees of freedom [5]

$$\nu_1 = \nu - 2N + 2, \tag{13}$$

where ν is the number of degrees of freedom of the spectral matrix in (9).

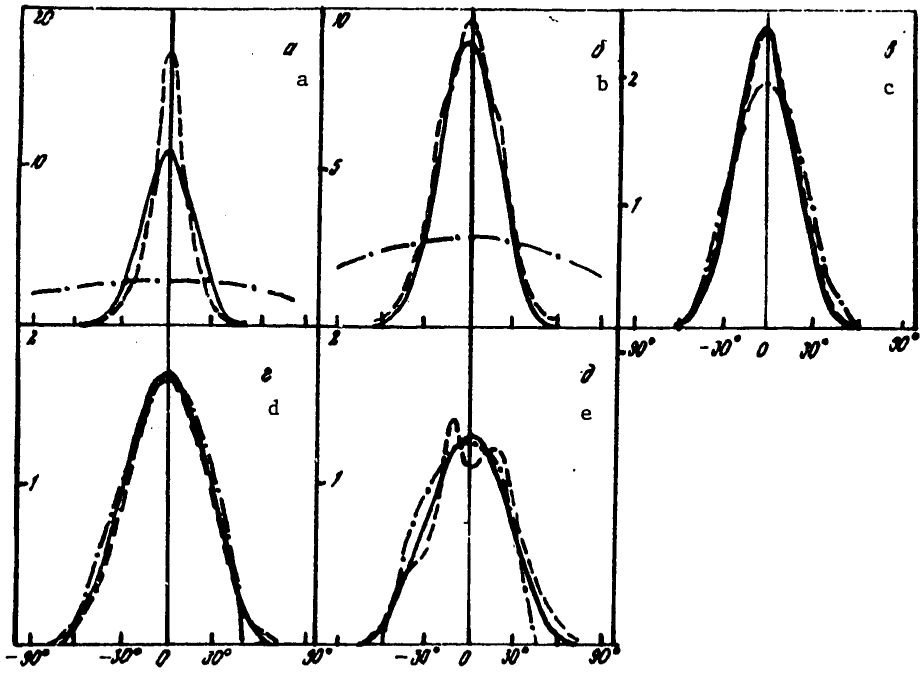

Fig. 2. Evaluations of models of angle spectrum: --- MPM; _._ Barber method; a) $\cos^{12}\theta$, k = 0.13 m^{-1}; b) $\cos^{8}\theta$, k = 0.13 m^{-1}; c) $\cos^{8}\theta$, k = 0.50 m^{-1}; d) $\cos^{4}\theta$, k = 0.50 m^{-1}; e) $\cos^{4}\theta$, k = 0.64 m^{-1}.

Experimental Results

The measurements were made at the marine experimental polygon Marine Hydrophysical Institute Ukrainian Academy of Sciences in the Black Sea. Capacitance-type string wave recorders were used for continuous registry of the

rise in the wave surface at several points [6]. They were attached on two stationary masts set up in the open part of the sea at a depth of 15 m at a distance of 300 m from the shore.

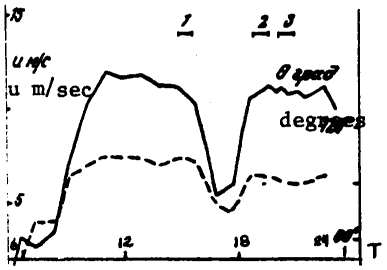

Fig. 3. Wind characteristics at time of observations: ___ velocity; --- direction; -- observation periods.

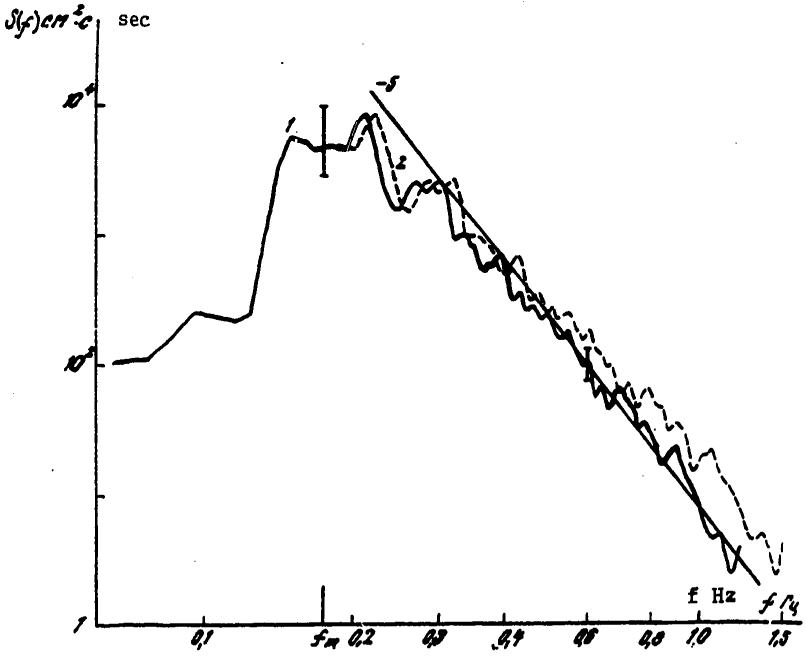

Fig. 4. Frequency spectra of wind waves: 1) spectrum averaged from five records of series 1; 2) spectrum without correction for current velocity. The straight line "-5" indicates $s(f) \sim f^{-5}$; the vertical segments represent the 95% percent confidence intervals in different frequency ranges.

We simultaneously registered wind velocity and direction at a height of 10 m and the horizontal and vertical components of the velocity of water movement under the surface of the waves. The velocity components were measured using reversing orbital velocity sensors mounted on these same masts.

Then we examined the results of detailed processing of three series of measurements obtained under quite stable wind conditions. The wind velocity and direction and also the periods of the measurements are shown in Fig. 3. The surface current at the time of the measurements was monitored and was about 0.3 m/sec. The collected data were processed using spectrum analysis programs. The length of the records was 1,500 points with a discreteness of 0.25 sec.

The frequency spectrum of waves S(f), averaged for five records from one of the series of measurements, is shown in Fig. 4. The equivalent number of degrees of freedom of the averaged spectrum varies from 20 in the region of the spectral density maximum to 100 for frequencies greater than 0.5 Hz, depending on the value of the coherence between surface rise signals. The wind waves regime under stipulated conditions (dimensionless duration $\tilde{T} = T \cdot g/u \simeq 2 \cdot 10^4$ and rough evaluation of dimensionless fetch $\tilde{x} = x \cdot g/u^2 \sim 10^3$-$10^4$) can be considered steady.

The influence of the mean current is important in the high-frequency region and is determined by the Doppler effect

$$\omega_1 = \omega + k V \cos \alpha , \tag{14}$$

where ω_1 is the cyclic frequency in a fixed reckoning system; ω is the frequency in a reckoning system moving with the velocity V; α is the angle between the direction of the wave and current. In a general case with transition from the spectrum $S(\omega_1)$ to $S(\omega)$ it is necessary to take into account the three-dimensional nature of the wind waves, that is, the type of the angle spectrum. However, as will be seen, the experimental evaluations of the angular distribution function are quite narrow and no additional correction for expression (14) is required for them.

The spectrum shown in Fig. 4 was constructed with expression (14) taken into account. The change in the S(f) spectrum as a result of allowance for corrections for the mean current is shown for series 1, where the dashed line denotes the wave spectrum obtained as a result of processing of the initial records. It can be seen that the influence of the current is important at frequencies $f \geqslant 0.4$-0.5 Hz: the spectral density level decreased by several times, as a result of which the S(f) slope was close to f^{-3}.

The MPM evaluations of the $F(\vec{k},\omega)$ spectra for the series of observations 1, 2, 3 were obtained in the range 0.15-0.45 Hz. It was found that all the spectra have very close directions of the energy maxima θ_0 which coincide

with the wind direction. The scatter of angles in the entire frequency band does not exceed ±10°. This is a result and confirmation of the stability of the wave field during the measurements. For a detailed study of the behavior of $F(\vec{k}, \omega)$ in frequency and wave number space it is necessary, in addition to a high resclution with respect to wave numbers, to ensure a quite high resolution in frequency. Otherwise there will be an infiltration of spectral energy from the frequency region into the wave number region. Due to the limited band for averaging of the cross-spectra Δf the band of averaging of evaluations $F(\vec{k}, \omega)$ for wave numbers Δk even in the case of infinite spatial resolution of the array of wave recorders (in the case of a dispersion relationship $\omega^2 = gk$) is

$$\Delta k = \frac{8\pi^2}{g} f \Delta f . \qquad (15)$$

The band Δf was selected equal to 0.01 Hz. Therefore, in the range of frequencies 0.15-0.45 Hz Δk was 0.012-0.036 m^{-1}. This resolution was adequate for determining the position of the spectral maximum $F(\vec{k}, \omega)$. A discussion of the deviations from the linear dispersion expression $\omega^2 = gk$ is beyond the framework of this study. We only note that the experimental results agree well with the theoretical dispersion curve to the doubled frequency of the spectral peak f_m.

The normalized angular distribution functions for the mentioned frequencies with double averaging (using adjacent frequencies in the range ±0.03 Hz and using three series of measurements) are given in Fig. 5,a,b. For these evaluations the equivalent number of degrees of freedom according to (13) is approximately equal to 70.

Figure 5 shows that the angular energy distributions are extremely narrow. In the region of the spectral peak they agree with the evaluation $\cos^{12}\theta$ (Fig. 5,a). There is a tendency to a broadening of the angular spectrum approximately to $\cos^6\theta$ with an increase in frequency.

In a linear approximation the frequency-angle spectrum is usually determined as

$$\chi(\omega, \theta) = S(\omega) \cdot A(\omega) K(\omega, \theta), \qquad (16)$$

where the normalization condition is

$$\int_0^{\infty} \int_{-\pi}^{\pi} A(\omega) \cdot K(\omega, \theta) d\omega d\theta = 1;$$

$S(\omega)$ is the frequency spectrum; $K(\omega, \theta)$ is a function describing the energy distribution of wind waves in the direction θ. Most frequently it is assumed that

$$K(\omega,\theta)=\begin{cases}\cos^{n(\omega)}(\theta-\theta_0), & |\theta-\theta_0|\leq\frac{\pi}{2}\\ 0, & |\theta-\theta_0|>\frac{\pi}{2}.\end{cases} \tag{17}$$

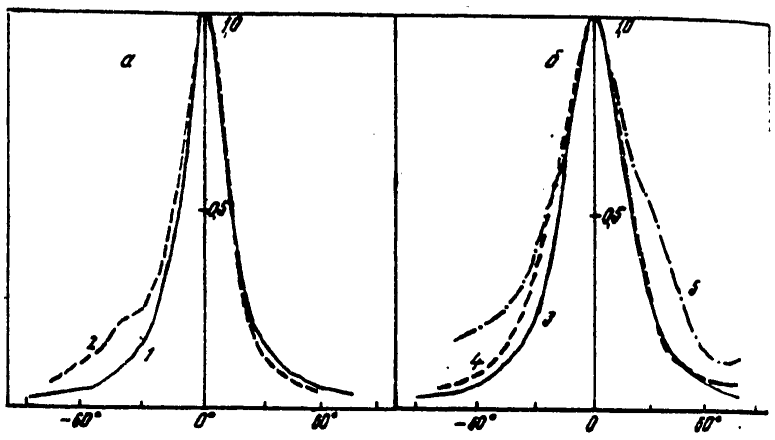

Fig. 5. Experimental evaluations of the angular distribution functions for the energy of wind waves at the frequencies (Hz): 1) 0.175; 2) 0.37; 3) 0.26; 4) 0.32; 5) 0.43.

The evaluations $k(\omega, \theta)$, obtained in our measurements, agree qualitatively with the results of other researchers [1, 7-9]. The general pattern for evaluations of angular spectra in these studies is a broadening of the angular distribution of energy with an increase in frequency. The authors of [7, 8] propose the approximation

$$K(\omega,\theta)\sim\left(\cos\frac{\theta-\theta_0}{2}\right)^{2S}, \tag{18}$$

where S is a decreasing function of frequency. The dependence of the angular distribution of energy on frequency was also obtained in [9] in the form

$$S=11{,}5\left(\frac{2\pi fu}{g}\right)^{-2{,}5} \qquad \text{for } f>f_m. \tag{19}$$

Here the S value is dependent not only on f, but also on the wind velocity u or on the frequency of the spectral peak f_m.

In a comparison of the approximations (17) and (18) it must be taken into account that they coincide with $n\simeq 0.46$ S. According to the evaluations of different authors, the n value varies from 8 to 1 in dependence on the stage of wave development [1], which is considerably broader than

our evaluations. For example, with a wind velocity of 11 m/sec and f_m = 0.175 Hz the S value from expression (19) is equal to 10, that is, $n \simeq 4-5$. The discrepancy in the evaluation of the width of the angle spectra is associated both with the resolution of the used methods and with the dependence of the angle distribution of energy on stability of the wind field. For a less uniform wind the angular distribution will naturally be broader.

A knowledge of the angular distribution of wave energy is of great interest for practical purposes. The predominant part of the energy of wind waves is concentrated in the region $f \leqslant 2f_m$. According to our data, the angular distribution function averaged in this frequency band for all measurement series is approximated best of all by expression (17) with n = 10 and the A value in (16) is equal to 1.294.

It is interesting to compare the results with the conclusions from the theory of the resonance mechanism of wave generation [13]. According to this model, in the case of a constant wind strength and direction the spectral density must be maximum in two narrow regions in the directions $\theta_m = \pm \arccos(c/u)$, where c is phase velocity; u is mean wind velocity. For our conditions the values of the resonance angles θ_m, determined for the region of the spectral maximum, must be a value ±20-35°. Figure 8 shows that the width of the angular distribution of energy is substantially less than the values predicted by theory and no double peaks appear in the angle spectra.

BIBLIOGRAPHY

1. Davidan, I. N., Lopatukhin, L. I., Rozhkov, V. A., VETROVOYE VOLNENIYE KAK VEROYATNYY GIDRODINAMICHESKIY PROTSESS (Wind Waves as a Probable Hydrodynamic Process), Leningrad, Gidrometeoizdat, 1978, 288 pages.

2. Kozubskaya, G. I., Konyayev, K. V., "Adaptive Spectral Analysis of Random Processes and Fields," IZV. AN SSSR, FAO (News of the USSR Academy of Sciences, Physics of the Atmosphere and Ocean), 13, No 1, pp 61-71, 1977.

3. Yefimov, V. V., Kulikov, Ye. A., "Use of the Method of Adaptive Evaluation of Spatial-Temporal Spectra in Analysis of Trapped Waves," IZV. AN SSSR, FAO, 14, No 7, pp 748-756, 1978.

4. Yefimov, V. V., Solov'yev, Yu. P., Khristoforov, G. N., "Experimental Checking of Phase Velocity of Propagation of the Spectral Components of Sea Wind Waves," IZV. AN SSSR, FAO, 8, No 4, pp 435-446, 1972.

5. Keypon, Gudmen, "Distribution of Probability of Evaluations of a Spatial-Temporal Spectrum," TIIER [Expansion Unknown], 58, No 11, pp 81-83, 1970.

6. Yefimov, V. V., Sizov, A. A., Khristoforov, G. N., "Wave Recorders With a Coaxial Capacitive Sensor," METODIKA I APPARATURA DLYA GIDROFIZICHESKIKH ISSLEDOVANIY (Methods and Instrumentation for Hydrophysical Research), Kiev, "Nauk. Dumka," pp 97-101, 1969.

7. Longuet-Higgins, M. S., Cartwright, D. E., Smith, N. D., "Observations of the Directional Spectrum of Sea Waves Using the Motions of the Floating Buoys," PROC. CONF. OCEAN WAVE SPECTRA, New York, Prentice-Hall, pp 111-136, 1963.

8. Ewing, J. A., "Some Measurements of the Directional Wave Spectrum," J. MAR. RES., 27, No 2, pp 163-171, 1969.

9. Mitsuyasu, H., et al., "Observations of the Directional Spectrum of Ocean Waves Using a Clover-Leaf Buoy," J. PHYS. OCEAN, No 4, pp 750-760, 1975.

10. Capon, J., "High-Resolution Frequency - Wave Number Spectrum Analysis," PROC. IEEE, 57, pp 1408-1418, 1969.

11. Davis, R. E., Rogier, L. A., "Methods for Estimating Directional Waves Spectra from Multielement Arrays," J. MAR. RES., 35, No 3, pp 453-477, 1977.

12. Barber, N. F., "The Directional Resolving Power of an Array of Wave Recorders," PROC. CONF. OCEAN WAVE SPECTRA, N. Y., Prentice-Hall, pp 137-150, 1963.

13. Phillips, O. M., "On the Generation of Waves by Turbulent Wind," J. FLUID MECH., 2, pp 417-445, 1957.

[351-5303]

5303
CSO: 1865

UDC 551.463.6

THERMAL STATE OF THE COLD SKIN LAYER

Sevastopol' MORSKIYE GIDROFIZICHESKIYE ISSLEDOVANIYA in Russian No 3, 1979 pp 105-112

[Article by V. N. Kudryavtsev and G. L. Luchnik]

Abstract: The article, within the framework of a very simple analysis of a laminar sublayer under the free surface of a cooling fluid, determines the relationship between the heat flow through the free surface and the dynamic velocity at which a change in the thermal state of the sublayer occurs. It is shown that with a definite value of the dynamic velocity in the thin subsurface layer there is a transition from free to forced convection. This leads to a different functional dependence of the mean temperature drop on external parameters. A comparison of the theoretical value of critical velocity with the experimental value obtained in [2] is given.

[Text] The use of remote research methods has given rise to interest in the characteristics of the temperature field of the free ocean surface T^s. A characteristic of T^s is that it is different from the temperature of the underlying well-mixed layer T^0. The entire temperature drop from tenths of a degree to a degree is concentrated in several millimeters under the free surface, in the sublayer of molecular thermal conductivity. Sometimes this thermal sublayer is called the temperature skin layer of the ocean [4]. Allowance for this layer is necessary both in an investigation of interaction between the ocean and the atmosphere and in an investigation of physical processes by the methods of remote sensing of the ocean.

The phenomena transpiring in the cold skin layer are very complex with respect to their internal mechanism and therefore for the time being it is difficult to describe them within the framework of the general hydrodynamics of the upper boundary layer of the ocean.

The article gives a parameterization of the mean temperature drop $\overline{\Delta T} = \overline{T^s} - \overline{T^0}$ in dependence on the set of characteristics of the near-water layer of the atmosphere and the upper mixed layer of the ocean. A series of laboratory and field experiments has been devoted to this problem [1-7]. Two cases are considered in the parameterization of the mean temperature drop in the skin layer: the skin layer under conditions of forced and under conditions of free convection.

For the first case in [7], assuming that the processes at the free surface are similar to processes at a smooth hard wall, it is assumed that

$$\overline{\Delta T} = \lambda' \frac{\nu}{\varkappa} q V_*^{-1}, \qquad (1)$$

where q is the heat flow through the surface; ν, $\varkappa$ are the kinematic coefficients of molecular viscosity and thermal conductivity respectively; V_* is dynamic velocity in the water; λ is an empirical constant. This expression is a corollary of the assumption that the entire temperature drop is concentrated in the layer $\delta_T \sim \nu \cdot V_*^{-1}$, where the heat transfer has a molecular character. Expression (1) has found convincing experimental confirmation under both real and under laboratory conditions [1, 6, 7].

In the case of free convection (in the absence of a wind over the surface of a cooling fluid), when the Rayleigh number of sufficiently large, the temperature drop is determined by the expression [1, 5, 8]

$$\overline{\Delta T} = -A^{-3/4} (g\alpha \varkappa^2/\nu)^{-1/4} (-q)^{3/4}, \qquad (2)$$

where $g\alpha$ is the buoyancy parameter; A is a constant; $q < 0$.

However, in a laboratory experiment [2] it was established that the parameterization of $\overline{\Delta T}$ by the expression (2) is also correct in the range of wind velocities $0 \rightarrow U^{cr}$. In the neighborhood of U^{cr} there is a jumplike change in the $\overline{\Delta T}$ value and with $U > U^{cr}$ the temperature drop in the sublayer of molecular thermal conductivity is determined by formula (1).

The principal purpose of this study is an attempt to determine the critical values of the parameters at the ocean-atmosphere boundary at which there is a change in the thermal state of the cold skin layer.

We will assume that the transfer processes at the free surface in the sea have an intermittent character, that is, the viscous sublayer and the sublayer of molecular thermal conductivity are subject to spatial and temporal destruction and injection into the turbulent flow. Then locally [in a coordinate system moving with surface velocity] in the time interval between successive destructions the temperature distribution in the sublayer will be described by the equation

$$\frac{\partial T}{\partial t} = \varkappa \frac{\partial^2 T}{\partial z^2} \tag{3}$$

with the initial and boundary conditions

$$T(0,z) = T^0, \quad \frac{\partial T}{\partial z}(t,0) = -q/\varkappa = const. \tag{3a}$$

The solution of equation (3) under the conditions (3a) has the form

$$T(z,t) - T^0 = \frac{2q\sqrt{\varkappa t}}{\varkappa}\left[\frac{1}{\sqrt{\pi}} e^{-\zeta^2} - \zeta \operatorname{erfc} \zeta\right], \tag{4}$$

where

$$\zeta = z/2\sqrt{\varkappa t}.$$

We will introduce the probability density function p(t) for the periods of destruction of the laminar sublayer, that is, the probability that the destruction of the laminar sublayer occurs in the interval t - t + dt, where time is reckoned from the preceding destruction. It is obvious that p(t) must satisfy the condition

$$\int_0^\infty p(t)\, dt = 1.$$

Then the mean temperature $\overline{T}(z)$ in the sublayer of molecular thermal conductivity will be written in the form

$$\overline{T}(z) = \int_0^\infty p(t) \frac{1}{t} \int_0^t T(z,t')\, dt'\, dt. \tag{5}$$

With (4) taken into account the expression for $\overline{\Delta T} = \overline{T}^s - \overline{T}^0$ assumes the form

$$\Delta T = \int_0^\infty p(t) \frac{1}{t} \int_0^t \frac{2q\sqrt{\pi \varkappa t'}}{\pi \varkappa} dt'\, dt = \frac{q}{\varkappa}\sqrt{\pi \varkappa t_*}\, \frac{4}{\partial \pi} \int_0^\infty \tilde{p}(\tau)\sqrt{\tau}\, d\tau, \tag{6}$$

where t_* is the mean lifetime of the laminar sublayer; $\tau = t/t_*$ and $\tilde{p}(\tau) = t_* p(t_*, \tau)$ is dimensionless time and the probability density function. We note that the approach considered above is similar to the method proposed in [11]. Equation (6) is the fundamental expression in this study.

Now we will discuss the possible reasons for the nonstationary nature of the laminar sublayer. In our opinion, there are two: local dynamic and convective instability.

We will examine the first reason for the nonstationary character. We will assume that there is an analogy of the processes in the viscous sublayers at the free surface and at the smooth rigid wall. In this case quite small wind velocities are considered so that it is possible to neglect the destruction of the viscous sublayer by the collapse of surface waves. The possibility of such an analogy was pointed out in a review by Saunders [4].

We note that the proposed analogy plays an important role in the subsequent analysis and its imperfections can probably lead to somewhat different results.

Visual investigations of the structure of the viscous sublayer of the flow at the smooth rigid wall indicated its nonuniform spatial-temporal structure [9, 10]. The local dynamic instability of longitudinal eddy formations leads to ejection of part of the fluid from the viscous sublayer. The mean interval between two successive "ejections" is determined by the expression [9]

$$t_*^g = c \cdot \nu \cdot V_*^{-2}, \tag{7}$$

where C is some constant. The time t_*^g determines the characteristic period of the viscous phase, ending in the destruction of the sublayer due to the instability of dynamic origin.

The second reason for the nonstationary character can be the convective instability of local cold (and accordingly, heavy) elements of the laminar sublayer. In actuality, whatever may be the nature of the destruction, in the subsequent laminar phase the temperature distribution is described by expression (4). If, adhering to the model [8], we introduce the local Rayleigh number

$$Ra(t) = \frac{g\alpha \Delta T \delta_T^3}{x\nu} = \frac{g\alpha \left[\frac{2}{\sqrt{\pi}} q x^{-1} \sqrt{xt}\right]\left[\frac{2}{\sqrt{\pi}}\sqrt{xt}\right]^3}{x\nu}, \tag{8}$$

then during cooling from above the thickness of the thermal boundary layer

$$\delta_T = \frac{2}{\sqrt{\pi}}\sqrt{xt}$$

and the temperature drop

$$\Delta T = \frac{2}{\sqrt{\pi}} q x^{-1} \sqrt{xt}$$

will increase until at the time t_*^k the Ra number reaches some critical value Ra^{cr}, after which the fluid is suddenly detached as a discrete element. The time t_*^k is determined from expression (8)

$$t_*^k = \left(\frac{Ra^{kp}}{16/\pi^2}\right)^{1/2} \left(\nu/g\alpha\right)^{1/2} q^{-1/2} \tag{9}$$

and characterizes some mean period of nonstationarity of the laminar sublayer associated with the mechanism of local convective instability. The nonstationarity mechanisms considered above are responsible for the destruction and injection of the laminar sublayer into the underlying region. Which of them will be decisive is dependent on the relationship of the times t_*^k and t_*^g. If $t_*^g < t_*^k$, there is a "blocking" of convective instability by a mechanism of a dynamic character, that is, in the limits of the viscous phase $0 - t_*^g$ of the cyclic process the formation of an unstable thermal

is impossible. On the other hand, when $t_*^k < t_*^q$ there is a "blocking" of the local dynamic instability of the viscous sublayer. In this case in the interval 0 - t_*^q there can be formation of convective instability and ejection of a thermal can lead to disruption of local conditions (in particular, smoothing-out of the peaked velocity profile in the viscous sublayer) for development of dynamic instability of the viscous sublayer. Equating the times t_*^q, t_*^k, with (9) and (7) taken into account, we determine some critical dynamic velocity

$$V_*^{cr} = \frac{2}{\sqrt{\pi}} Ra^{1/4} c^{1/2} (\nu g\alpha)^{1/4} q^{1/4}. \qquad (10)$$

Thus, for the characteristic period t we obtain

$$t_* = \begin{cases} \frac{Ra^{1/2}}{4\pi} (\nu / g\alpha)^{1/2} q^{-1/2} & \text{with } V_* < V_*^{cr}, \\ c\nu V_*^{-2} & \text{with } V_* > V_*^{cr}. \end{cases} \qquad (11)$$

Substituting (1) into (6), we obtain

$$W = \begin{cases} \lambda_1 (g\alpha \varkappa^2 / \nu)^{-1/4} q^{3/4} & \text{with } V_* < V_*^{cr}, \qquad (12a) \\ \lambda_2 (\nu / \varkappa)^{1/2} q V_*^{-1} & \text{with } V_* > V_*^{cr}, \qquad (12b) \end{cases}$$

where

$$\lambda_1 = Ra^{1/4} \frac{2}{3} \int_0^\infty \tilde{\rho}_1(\tau) \sqrt{\tau}\, d\tau, \quad \lambda_2 = c^{1/2} \frac{4}{3\sqrt{\pi}} \int_0^\infty \tilde{\rho}_2(\tau) \sqrt{\tau}\, d\tau,$$

and $\tilde{\rho}_1$ and $\tilde{\rho}_2$ are the corresponding density distribution functions for the different regimes considered here.

As the initial parameters we will use $\varkappa = 1.25 \cdot 10^{-3}$ cm^2·sec^{-1}, $\nu = 10^{-2}$ cm^2·sec^{-1}, $g\alpha = 0.25$ cm·sec^{-2}·degree^{-1}, Ra = 64 [3], $c = 5 \cdot 10^2$.

Since we do not have information making it possible to validate the introduction of some specific density distribution function, we will compute λ_1 and λ_2 for some models p(t) satisfying the conditions p(t) = 0 with t = 0 and $p(t) \to 0$ with $t \to \infty$.

As an example we will consider the following density distributions:

a) gamma distribution

$$p(t) = \frac{\beta^\gamma}{\Gamma(\gamma)} t^{\gamma-1} e^{-\beta t}, \qquad t > 0, \quad \beta > 0, \quad \gamma > 1.$$

Here $\gamma/\beta = t_*$ is the mathematical expectation of the t value; γ/β_2 is the t dispersion; $\Gamma(\gamma)$ is the gamma function. Then

$$\tilde{\rho}(\tau) = \frac{\gamma^{\gamma}}{\Gamma(\gamma)} \tau^{\gamma-1} e^{-\gamma\tau} ;$$

b) Poisson distribution

$$\rho(t) = \frac{t}{t_*^2} e^{-t/t_*}, \quad t > 0 \quad \text{or} \quad \tilde{\rho}(\tau) = \tau e^{-\tau};$$

c) log-normal distribution law

$$\rho(t) = \frac{1}{\sqrt{2\pi}} \frac{\lg e}{\sigma t} e^{-\frac{1}{2}\left(\frac{\lg t - \lg t_*}{\sigma}\right)^2}, \quad t > 0,$$

where σ^2 is the dispersion, that is, the mathematical expectation of the value $(\lg t - \lg t_*)^2$. In this case

$$\tilde{\rho}(\tau) = \frac{1}{2\sqrt{\pi}} \frac{\lg e}{\sigma\tau} e^{-\frac{1}{2}\left(\frac{\lg \tau}{\sigma}\right)^2};$$

d) degenerate distribution

$$\rho(t) = \delta(t - t_*) = \begin{cases} 0 & \text{when } t \neq t_*, \\ \infty & \text{when } t = t_*, \end{cases}$$

Or

$$\tilde{\rho}(\tau) = \delta(\tau - 1).$$

Then for each of the distributions the integral

$$I = \int_0^{\infty} \tau^{\frac{1}{2}} \tilde{\rho}(\tau) d\tau$$

and the coefficients λ_1 and λ_2 will be:

a) $$I = \gamma^{-\frac{1}{2}} \cdot \frac{\Gamma\left(\gamma + \frac{1}{2}\right)}{\Gamma(\gamma)}, \qquad I \to 0{,}89, \ \lambda_1 \to 1{,}7, \ \lambda_2 \to 14{,}7$$

in this case $I \to 0.89$, $\lambda_1 \to 1.7$, $\lambda_2 \to 14.7$ with $\gamma \to 1$ and $I \to 1$, $\lambda_1 \to 1.9$, $\lambda_2 \to 16.5$ with $\gamma \to 0$;

b) $I = 1.33$, $\lambda_1 = 2.5$, $\lambda_2 = 22$;

c) $I = e^{\frac{\sigma^2}{8 \lg^2 e}}$,

in this case $I \to 1$, $\lambda_1 \to 1.9$, $\lambda_2 \to 16.5$ with $\sigma \to 0$, and, for example, $I \simeq 2$, $\lambda_1 = 8.8$, $\lambda_2 = 33$ with $\sigma = 1$, which corresponds to a rather broad (of the order 10 t_*) t scatter;

d) $I = 1$, $\lambda_1 = 1.9$, $\lambda_2 = 16.5$.

The cited evaluations show (except for the case "c," where what is known to be a large dispersion was taken) a relatively small sensitivity of the coefficients λ_1 and λ_2 to the form of the density distribution p(t).

The experiments give $\lambda_1 = 2.8$ [1] and $\lambda_2 = 14-28$ with a mean value 20 [7]. We note that in [7] the author experimentally determined the value $\lambda_2^1 = \lambda_2 (\nu/\varkappa)^{-1/2}$, where the values $\lambda_2^1 = 5-10$ are given with a mean value 7.

Finally, we will evaluate the critical dynamic velocity. With the adopted initial parameters it follows from (10) that $V_*^{cr} = 2q^{1/4}$.

For comparison with the results of the experiment reported in [2] we will express V_* through the dynamic velocity in the air U_*.

As a result, $U_*^{cr} = 2(\rho_w/\rho_a)^{1/2} q^{1/4}$. With $\rho_w/\rho_a = 0.77 \cdot 10^{-3}$, $q = 10^{-2}$ degree·cm·sec^{-1}. We obtain $U_*^{cr} = 17.5$ cm·sec^{-1}, which agrees with $U_*^{cr} \sim$ 20-25 cm·sec^{-1}, found experimentally. The evaluation U_*^{cr} was made using the mathematical expectation t_* and is not dependent on the form of p(t).

Thus, within the framework of a very simple analysis it is possible to determine the relationship between the dynamic velocity and the heat flow with which there is a change in the thermal state of the cold skin layer. With $U_* < U_*^{cr}$ the temperature drop is found from (12a); in the opposite case -- from (12b). As can be seen from (6), the different behavior of $\overline{\Delta T}$ is determined by the dependence of the mean "lifetime" t_* of the laminar sublayer on the type of its destruction: either convective (9) or dynamic (7).

BIBLIOGRAPHY

1. Ginzburg, A. I., Fedorov, K. N., "Cooling of Water During Free and Forced Convection," IZV. AN SSSR, FAO (News of the USSR Academy of Sciences, Physics of the Atmosphere and Ocean), 14, No 1, pp 79-87, 1978.

2. Ginzburg, A. I., Fedorov, K. N., "Thermal State of the Boundary Layer of Cooling Water With Transition from Free to Forced Convection," IZV. AN SSSR, FAO, 14, No 7, pp 778-785, 1978.

3. Ginzburg, A. I., Fedorov, K. N., "The Rayleigh Critical Boundary Number During the Cooling of Water Through a Free Surface," IZV. AN SSSR, FAO, 14, No 4, pp 433-436, 1978.

4. Saunders, P. M., "The Skin Temperature of the Ocean. A Review," MET. SOC. ROY. SCI., Liege, VI, pp 93-99, 1974.

5. Katsaros, K. B., Liu, T., Businger, J. A., Tillman, J. A., "Heat Transport and Thermal Structure in the Interfacial Boundary Layer Measured in an Open Tank of Water in Turbulent Free Convection," J. FLUID MECH., 83, No 2, pp 311-335, 1976.

6. Hill, H., "Laboratory Measurement of Heat Transfer and Thermal Structure Near an Air-Water Interface," J. PHYS. OCEANOGR., 2, pp 190-198, 1972.

7. Saunders, P. M., "The Temperature at the Ocean-Air Interface," J. ATMOS. SCI., 24, No 2, pp 269-273, 1967.

8. Howard, L. N., "Convection at High Rayleigh Number," PROC. 11th INT. CONGR. APPL. MECH., Munich, pp 1374-1389, 1962.

9. Kline, S. J., Reynolds, W. S., Schraub, F. A., Runstadler, P. W., "The Structure of the Turbulent Boundary Layer," J. FLUID MECH., 30, 4, pp 741-768, 1967.

10. Corino, E. R., Brodkey, R. S., "A Visual Investigation of the Wall Region in Turbulent Flow," J. FLUID MECH., 37, 1, pp 1-30, 1969.

11. Liu, W. T., Businger, J. A., "Temperature Profile in the Molecular Sublayer Near the Interface of a Fluid in Turbulent Motion," GEOPH. RES. LETTER, 2, No 9, pp 403-404, 1975.

[351-5303]

5303
CSO: 1865

UDC 551.466.3

MANIFESTATION OF NONLINEARITY OF SURFACE SEA WAVES IN STATISTICAL AND SPECTRAL CHARACTERISTICS

Sevastopol' MORSKIYE GIDROFIZICHESKIYE ISSLEDOVANIYA in Russian No 3, 1979 pp 113-124

[Article by G. N. Khristoforov, V. Ye. Smolov and A. S. Zapevalov]

Abstract: Data from experimental investigations of surface sea waves in the presence of a weak wind are examined. There was found to be a special type of variability of structure, expressed in the fact that the profiles of short-period waves in some time interval become more "trochoidal," whereas in other intervals they are more "sinusoidal." This is reflected in the statistical characteristics of the distributions (such as asymmetry and excess); in the spectra it is possible to trace changes in the specific content of the harmonics of these short-period waves. Such a variability of structure can be attributed to nonlinear interactions in waves, in particular, the interaction between surface and internal waves.

[Text] 1. Introduction. In the theory of wind waves it is common to assume a Gaussian nature of the statistical structure of the wave-covered sea surface [1, 2]. Such an approach is undoubtedly justified in those cases when it is possible to neglect the high-frequency spectral region of sea waves. Nevertheless, investigations made in recent years have indicated that wind waves are characterized by weak nonlinear interactions and therefore cannot be regarded as purely Gaussian processes. In describing wave statistics use is made of Gram-Charlier series, for which a Gaussian distribution is obtained in the first approximation with the discarding of high-order terms [3, 10, 11].

According to available experimental data, for the surface rise in wind waves $\eta(t)$ the deviations of the distribution from a normal distribution are not great [4, 10]. During measurements in the Golfe du Lion [5]

at the time of a storm with a wind velocity 10-12 m/sec there were more significant deviations from a normal distribution (the asymmetry and excess of the empirical distributions attained values A = 0.3-0.6 and E = 0.5-1.5 respectively) than in the presence of weak winds when the energy of the wave field was determined for the most part by swell (in these cases A and E had small values of about 0.1). These results agree with the considerations presented above on the role of high-frequency (including nonlinear) components of the wave spectrum, but up to the present time the literature has contained no experimental data indicating a direct relationship between the manifestations of a nonlinear character of sea waves and deviations of the parameters of the distribution from a normal distribution. This article is an attempt at demonstrating the appearance of such effects observed under natural conditions.

2. Measurement method. It is well known that when there are weak and moderate winds at sea it is possible to observe sectors of wave-covered surface alternating with smoother sectors (for example, see [6, 12]). A distinguishing characteristic of the wave-covered sectors is the existence on them of short ripple waves having a relatively great steepness (sometimes even with whitecaps on the crests) which are propagated along the surface of longer swell waves, whereas in adjacent, calmer sectors the ripples appear more gently sloping. This makes it possible to evaluate the variability of the statistical characteristics of short waves, studying the surface structure in wave-covered and calm sectors respectively. that is, sectors with different wave steepness.

Our measurements were made in July 1977 in the experimental polygon of the Marine Hydrophysical Institute Ukrainian Academy of Sciences in the neighborhood of Katsiveli village using an automatic string wave recorder which makes it possible to register oscillations of the sea surface level with frequencies from 0.05 to 20-30 Hz [7]. Since the spectrum of the rise $S_\eta(f)$ at the high frequencies decreases rather steeply, in order to obtain information on short waves the full dynamic range of registry must be about 60-70 db. This was ensured by use of electronic active filters suppressing the low-frequency oscillations caused by the contribution of the main energy-carrying wave systems, but transmitting undistorted high-frequency components which have a relatively low energy.

The wave recorder was mounted on a stationary mast situated at a distance of 350 m from the shore at a depth of 15 m. The frequency-modulated signal of the wave recorder was transmitted through a cable to the shore, where it was subjected to demodulation, processed by means of filters and registered on an analog N338 recorder. The resulting records were used in forming series with a length N = 700-1100 readings each. The discreteness of Δt readout was selected in dependence on the filter used during registry. The programs for processing the data on an electronic computer included obtaining the statistical moments of the distribution (dispersion σ_η^2, asymmetry A, excess E), the autocorrelation functions and the power spectra. In constructing the spectrum in the region of the principal

energy-carrying frequencies we used wave records registered with filters having a linear characteristic curve at frequencies greater than 0.05 Hz (Δt = 0.2 sec). For an analysis of the short-wave parts of the spectrum during registry of the wave record we used filters transmitting signals with frequencies greater than 2 (Δt = 0.04 sec) and 5 Hz (Δt = 0.008 sec). In computing the spectra we used Tukey filtering windows. The number of degrees of freedom was 40-60 in all cases.

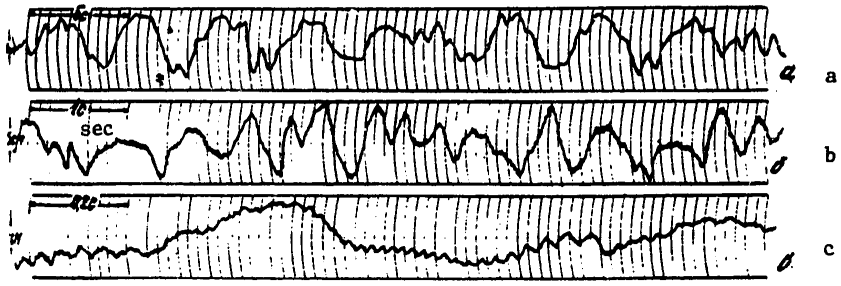

Fig. 1. Fragments of wave record registered using different filters in frequency bands: a) 0.05-30 Hz; b) 2-30 Hz; c) 5-30 Hz

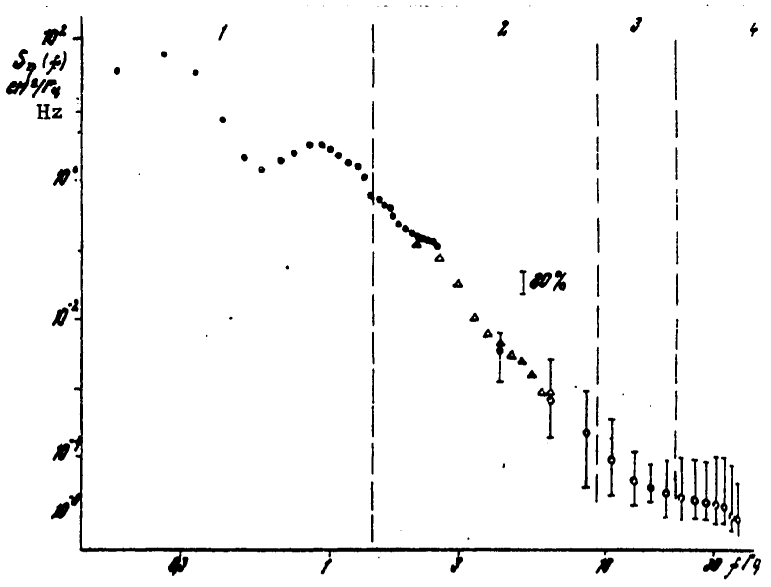

Fig. 2. Evaluations of spectrum of surface rise $S_{\eta}(f)$ on the basis of 14 wave records registered using different filters in frequency bands: filled circles -- first; triangles -- second; open circles -- third

3. Observational data. One of the graphic examples of variability of the statistical characteristics of short gravitational waves (ripples) is given by experimental data obtained under relatively uniform conditions in the course of one hour in the case of a small unstable wind whose velocity varied in the range from 1.5-2 to 3-4 m/sec.

Figure 1 shows fragments of wave records registered during this period and Fig. 2 shows the spectrum of the surface rise $S_\eta(f)$, constructed from these records. As a convenience in interpretation, the spectrum taking in the broad frequency region from 0.05 to 30 Hz has been broken down into several intervals: 1) fundamental energy-carrying oscillations; 2) short gravitational waves with periods less than 1-0.5 sec; 3) gravitational-capillary waves; 4) capillary waves.

The evaluations of spectral density $S_\eta(f)$ in Fig. 2 were obtained in the processing of 14 wave records by the method described above (also see [7]). In the second-fourth intervals vertical segments are used to designate the upper and lower values of the $S_\eta(f)$ evaluations, found using all the wave records. The greatest variability was present at frequencies greater than 5-8 Hz, where the spectral density varied in a range exceeding the 80% confidence interval.

Figures 1 and 2 show that during measurements at the sea surface there were several systems of waves. First there was a very gently sloping swell arriving from the open sea (period $T^{(1)} \approx 4.2$ sec, wave length $L^{(1)} \approx 30$ m, height $h^{(1)} \lesssim 25$ cm). Second, there was a local system of waves ($T^{(2)} \approx 1.2$ sec, $L^{(2)} \approx 2$-2.5 m, $h^{(2)} \leqslant 5$-10 cm). Third, there were short gravitational ripple waves ($T^3 \approx 0.5$, $L^{(3)} \approx 0.3$-0.5 m). Finally, on the wave records one could the most high-frequency components, relating to the third and fourth spectral intervals. In Figures 1,c and 3,a it can be seen clearly how on the surface of ripples, having periods of the order of 0.5 sec, there is propagation of capillary ripples, with a still higher frequency, arising during a brief "gusty" intensification of wind velocity from 2 to 4.5 m/sec (for this wave record we obtained high $S_\eta(f)$ values in the fourth interval).

Due to the fact that the spectral density level $S_\eta(f)$ at high frequencies changed in a wide range, during the observation period the state of the sea surface was far from saturation. Accordingly, in this case in describing the spectrum it is impossible to use the usually employed models of the spectra (such as the Phillips spectrum f^{-5} for gravitational waves, the spectrum f^{-4} for the third and the spectrum $f^{-1/3}$ for the fourth interval [3, 13]). The general tendency to a decrease in $S_\eta(f)$ in the second interval is close to $f^{-4.5}$, and in the third and fourth intervals the slope of the spectrum becomes less.

4. Nonlinear effects. One of the interesting characteristics of these wave records is that in their different sectors there are changes in the nature of the wave oscillations, having periods centered at 0.5 sec. Figure 3,

as an example, shows fragments of wave records selected in such a way that this type of structural variability is demonstrated. It can be seen that there was an alternation of sectors in which the wave oscillations had a "trochoidal" character (Fig. 3, a, c, e) with sectors of the record where the form of the oscillations became closer to "sinusoidal" (Fig. 3,b,d). We will examine this circumstance in greater detail.

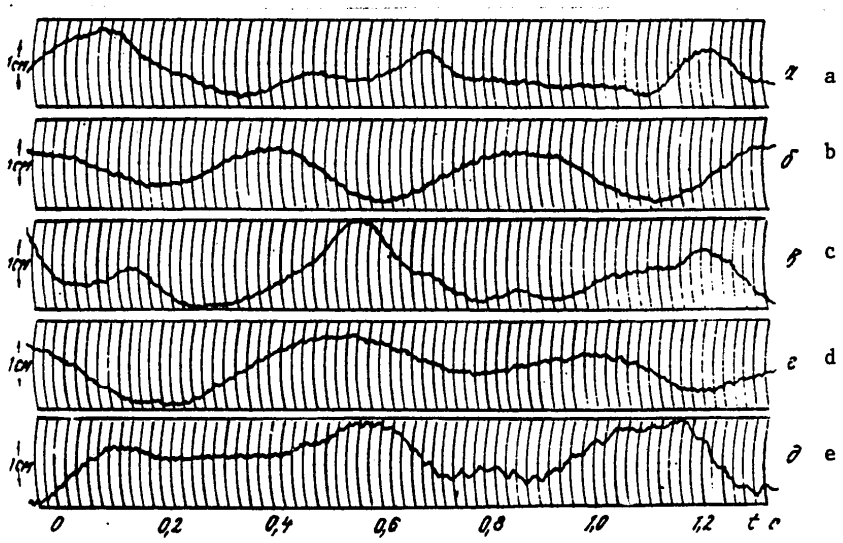

Fig. 3. Variability of short-period gravitational waves. The wave records were registered in the third frequency band at successive moments in time, separated by intervals of about several minutes.

As is well known, gravitational waves of finite amplitude at the surface of a fluid have sharper crests and more gently sloping bases in comparison with sinusoidal level oscillations in small-amplitude waves. This phenomenon is represented by a model of Stokes waves of finite amplitude in which the wave profile is represented in the form of a series

$$\eta = -a\cos kx + \frac{1}{2}\alpha a\cos 2kx - \frac{3}{8}\alpha^2 a\cos 3kx + \ldots, \qquad (1)$$

where a is wave amplitude; $k = 2\pi h/L$ is the wave number of the surface waves; $\alpha = ak$ is the steepness parameter ($\alpha = \pi h/L = \pi\delta$). Expression (1) shows that the deviation of the wave profile from sinusoidal is the stronger the greater the steepness of the wave δ. We note that with an accuracy to the third order of magnitude the profiles of Stokes waves and trochoids are identical [10]. Therefore, in this context the term "trochoidal" indicates the character of change of the wave profile. In order to shorten the writing of the expressions we will designate the "trochoidal" amd "sinusoidal" parts of the wave records as T and S structures respectively. Thus,

the appearance of a T structure can serve as an indicator of an increase in wave steepness (and accordingly, nonlinearity).

In the dynamics of surface waves an important role is played by nonlinear interactions, including internal, associated with an effect of finite amplitude. Thus, the investigations of Benjamin and Feir have shown that waves of a finite amplitude are characterized by nonlinearity, leading with time to their destruction [8, 14]. In the random field of wind waves the physical pattern is much more complex, but it is also characterized by internal relationships between the different components. The intensification of nonlinear interactions is accompanied by the disruption of the Gaussian character of the wave field. This should lead to an increase in the cumulants of the statistical distributions.

These qualitative reasonings help in understanding why the variability of statistical characteristics can serve as an indicator of the manifestation of nonlinear interactions in waves. In particular, it can be expected that the "trochoidality" and "sinusoidality" of wave oscillations is manifested somehow in the statistical characteristics. In actuality, as indicated by the data cited in the table, the asymmetry

$$A = (N\sigma_x^3)^{-1} \sum_1^N (x_i - \bar{x})^3,$$

excess

$$E = (N\sigma_x^4)^{-1} \sum_1^N (x_i - \bar{x})^4 - 3$$

and Cornu coefficient

$$K = N \left[\sigma_x^2 \left(\sum_1^N |x_i - \bar{x}| \right)^{-2} \right]$$

changed considerably in those cases when the nature of the wave record changed. The indicated A, E, K values indicate some deviations from a normal distribution (for normal distributions A = 0, E = 0, K = $\pi/2$). All the E evaluations fall in the region of negative values, which possibly is attributable to an inadequately deep suppression of the low-frequency components during signal filtering prior to registry. Except for this, the behavior of the A, E, K values was similar: for the T-structure their values were greater than for the S structure.

Despite the fact that on the wave record 3,e one can clearly see the high-frequency components (capillary ripples), A, E, K evaluations were obtained for it which fall in an intermediate interval in comparison with the evaluations for 3,a,c and 3,b,d. Evidently, the variability of the statistical characteristics is not so much associated with the presence of high-frequency components as with a change in their character. Thus, this makes it possible to judge what kind of oscillations predominate in the record.

The table also gives evaluations of the dispersion of wave oscillations in different frequency bands: (σ_η^2) in the band 2-30 Hz (energy of ripples with a period 0.5 sec); $(\sigma_\eta^2)_2$ in the band 4-9 Hz (corresponds approximately to the energy of the second, third and fourth harmonics of these ripples); $(\sigma_\eta^2)_3$ in the band 9-16 Hz (energy of components in the third interval); $(\sigma_\eta^2)_4$ in the band 16-30 Hz (energy of the components in the fourth interval). It can be seen from these data that the variability of the parameters $(\sigma_\eta^2)_3$ and $(\sigma_\eta^2)_4$ does not correspond to the nature of the variability of the A, E, K parameters. At the same time, the T structure differs from the S structure in having a higher level of content of harmonics in the spectrum.

The contribution of the nonlinear harmonics of the fundamental mode of the oscillation can be evaluated using the coefficient of the harmonics γ_S, representing the ratio of the amplitudes of the harmonic components to the amplitude of the fundamental mode. For example, for regular waves of finite amplitude, represented by expression (1),

$$\gamma_S = \frac{a_2 + a_3 + \dots}{a_1} = \alpha\left(\frac{1}{2} + \frac{3}{8}\alpha + \dots\right), \qquad (2)$$

from which it can be seen that with an increase in wave steepness the relative content of the harmonics increases. In the case of a continuous wave spectrum, to be sure, it is impossible to indicate precisely where specifically the contribution to spectral density is caused only by the harmonics and where it is caused by gravitational waves with the same frequency. However, if the T structure alternates with the S structure, it can be expected that some idea about this is given by the coefficient γ, similar in sense, which we will define as the square root of the ratio of the dispersion of the harmonics (that is, the dispersion $(\sigma_\eta^2)_2$, taken in the band 4-9 Hz, which approximately corresponds to the harmonics of waves of the fundamental mode, having periods of about 0.5 sec), to the dispersion of the waves of the fundamental mode.

$$\gamma = \left\{(\sigma_\eta^2)_2 \Big/ \left[(\sigma_\eta^2)_1 - (\sigma_\eta^2)_2 - (\sigma_\eta^2)_3 - (\sigma_\eta^2)_4\right]\right\}^{1/2}. \qquad (3)$$

In the last line of the table we have given the values of the γ coefficient; these show that for the T structure the specific content of harmonics is two or three times greater than for the S structure (although, to be sure, it cannot be assumed that the determined γ values correspond precisely to the relative level of the harmonic components).

Figure 4 shows the correlation between the statistical characteristics of the A, E, K distributions and the determined values of the coefficient for one and the same cases of measurement (for 11 series). Despite the scatter, it can be seen that higher γ values correspond to higher A, E, K values. This agrees with the assumption expressed above that there is a correlation between nonlinearity in waves and impairment in the Gaussian nature of the wave field.

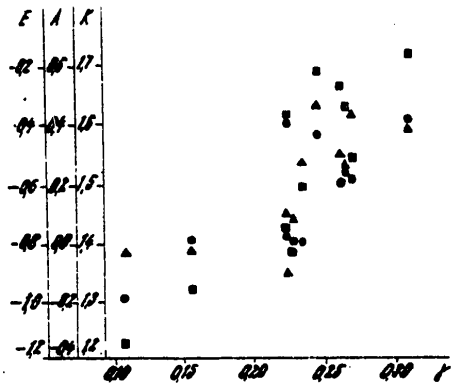

Fig. 4. Dependence of statistical characteristics of distribution on specific content of harmonics in spectrum: ▲ -- asymmetry; ■-- excess; ● -- Cornu coefficient

Table 1

Variability of Statistical Characteristics of Short-Period Components of Wave Field. Wind velocity $U_a \approx$ 2-4 m/sec; Total Dispersion of Wave Field $\sigma_\eta^2 = 17.2$ cm^2

Number of Wave Record in Fig. 3	a	b	c	d	e
Wind velocity, m/sec	1.5-2	1.5-2	2.2.5	2.25	4-4.5
Type of structure	T	S	T	S	T
Asymmetry, A	+0.38	-0.03	+0.45	-0.04	+0.10
Excess, E	-0.16	-0.96	-0.32	-1.15	-0.76
Cornu coefficient, K	1.00	1.40	1.52	1.31	1.44
Dispersion of ripples, 2 - 30 Hz, $(\sigma_\eta^2)_1$ cm^2	0.150	0.143	0.276	0.243	0.256
Dispersion of harmonics 4-9 Hz, $(\sigma_\eta^2)_2$ cm^2	0.013	0.003	0.018	0.003	0.012
Dispersion of HF components of third interval 9-16 Hz, $(\sigma_\eta^2)_3$ cm^2	0.0002	0.0002	0.0017	0.0003	0.0005
Dispersion of HF components of fourth interval 16-30 Hz, $(\sigma_\eta^2)_4$ cm^2	0.0003	0.0006	0.0005	0.0005	0.0014
Coefficient of harmonics	0.31	0.15	0.27	0.11	0.22

5. Physical interpretation. The collected data on the variability of the statistical characteristics of the distributions of the short-wave components of the spectrum in themselves still do not make it possible to draw any conclusion as to what physical mechanism leads to the appearance of a T structure alternating with an S structure. For such an analysis it is

evidently necessary to ensure monitoring of a considerably greater number of parameters than was done in our investigations. Nevertheless, since it can be seen from the table that changes in wind velocity exerted an influence for the most part on the components of the third and fourth intervals, it can be assumed that the variability of structure observed at lower frequencies was not associated with the direct influence of the air flow on the underlying surface, but with some other mechanism.

It is known that the form of the waves can be modified if the waves are propagated in a region of variable current velocity, since in this case there is an exchange of energy between the waves and the current [16, 17]. One of the special cases of such interaction is the interaction between surface and internal waves in the sea. Rather strong effects must be observed when there is coincidence of the phase velocity C_i of internal waves with the group velocity C_{go} of surface waves [9, 15]). Experimental investigations carried out in flumes [18] indicated that with such a "resonance" interaction between surface waves and internal waves the amplitudes and slopes of the surface waves can vary by a factor of 2-2.5.

It can be postulated that fluctuations of the γ coefficient observed during our measurements were caused by such a mechanism. In actuality, by comparing expression (2) and the tabulated data we find that the changes in γ by a factor of 2-3 were associated with changes in the steepness of waves having periods of about 0.5 sec. The group velocity of these waves is approximately 40 cm/sec, and this is rather close to the characteristic values of the phase velocity of propagation of the first modes of the internal waves in the shelf zone. Accordingly, the assumption made does not contradict the known data on the changes which can occur with surface waves during their interaction with internal waves. Sounder conclusions can be drawn, to be sure, only after carrying out investigations relating to different aspects of the problem as a whole.

Summary

1. When there is a weak wind the wave spectrum does not attain saturation, as a result of which there can be significant fluctuations of the spectral density level at the high frequencies. In the spectrum it is possible to discriminate the following wave systems: locally excited and arriving from other regions of the sea. Instability and wind gusts evidently exert an influence for the most part on the capillary spectral region (third and fourth spectral intervals).

2. The short-period ripples on the wave records can appear to be "troichoidal" (T structure) in the course of some time interval alternating with other intervals when the ripples appear "sinusoidal" (S structure).

3. The changes in the characteristics of short-period ripples can be judged from the change in the statistical coefficients of the A, E, K distributions. In addition, the T structure is characterized by a higher specific

content of harmonics in the spectrum, that is, a greater nonlinearity in comparison with the S structure.

4. It can be postulated that the observed variability in structure is caused by nonlinear interactions in the waves, such as the interaction of surface waves with currents and internal waves.

The authors express appreciation to Doctor of Physical and Mathematical Sciences V. V. Yefimov for discussion of the results of the study and useful advice.

BIBLIOGRAPHY

1. Krylov, Yu. M., SPEKTRAL'NYYE METODY ISSLEDOVANIYA I RASCHETA VETROVYKH VOLN (Spectral Methods for Investigation and Computation of Wind Waves), Leningrad, Gidrometeoizdat, 1966, 255 pages.

2. Glukhovskiy, B. Kh., ISSLEDOVANIYE MORSKOGO VETROVOGO VOLNENIYA (Investigation of Sea Wind Waves), Leningrad, Gidrometeoizdat, 1966, 284 pages.

3. Phillips, O. M., DINAMIKA VERKHNEGO SLOYA OKEANA (Dynamics of the Upper Layer of the Ocean), Moscow, "Mir," 1969, 267 pages.

4. Khristoforov, G. N., "On the Problem of Constructing Physical Models of the Upper Boundary Layer in the Ocean," MORSKIYE GIDROFIZICHESKIYE ISSLEDOVANIYA (Marine Hydrophysical Investigations), No 3, Sevastopol', pp 92-112, 1970.

5. Khristoforov, G. N., Zapevalov, A. S., Proshchenko, V. G., "Experimental Investigations of Structure and Variability of Temperature Fluctuations in the Upper Layer of the Sea," SOVETSKO-FRANTSUZSKIYE ISSLEDOVANIYA. VZAIMODEYSTVIYE ATMOSFERY I OKEANA (Soviet-French Investigations. Interaction Between the Atmosphere and Ocean), Sevastopol', Izd. MGI AN UkrSSR, pp 46-61, 1978.

6. La Fond, Ye. S., VNUTRENNIYE VOLNY. Ch. 1 (Internal Waves. Part 1), MORE (The Sea), Leningrad, Gidrometeoizdat, pp 346-373, 1965.

7. Khristoforov, G. N., Smolov, V. Ye., Zapevalov, A. S., "Measurement of the Spectrum of Sea Waves in a Broad Range of Scales," EKSPERIMENTAL'NYYE ISSLEDOVANIYA V MORE (Experimental Investigations at Sea), Sevastopol', Izd-vo MGI AN UkrSSR, pp 43-48, 1978.

8. Benjamin, T. B., "Instability of Periodic Trains of Waves in Nonlinear Systems With Dispersion," NELINEYNAYA TEORIYA RASPROSTRANENIYA VOLN (Nonlinear Theory of Wave Propagation), Translated from English, edited by G. I. Barenblatt, Moscow, "Mir," pp 83-104, 1970.

9. Phillips, O. M., "Interaction Between Surface and Internal Waves," IZV. AN SSSR, FAO (News of the USSR Academy of Sciences, Physics of the Atmosphere and Ocean), Vol 9, No 9, pp 954-961, 1973.

10. Kirsman, B., WIND WAVES, Prentice Hall, New York, 9, p 676, 1965.

11. Longuet-Higgins, M. S., "The Effect of Nonlinearities on Statistical Distributions in the Theory of Sea Waves," JOURNAL OF FLUID MECH., Vol 17, p 3, pp 459-480, 1963.

12. Perry, R. B., Schimke, G. R., "Large Amplitude Internal Waves Observed Off the Northwest Coast of Sumatra," JGR, Vol 70, No 10, pp 2319-2324, 1965.

13. Mitsuyasu, H., "Measurements of the High-Frequency Spectrum of Ocean Surface Waves," JOURNAL OF PHYSICAL OCEANOGRAPHY, Vol 7, No 6, pp 882-891, 1977.

14. Benjamin, T. B., Feir, J. E., "The Disintegration of Wave Trains on Deep Water. Part I, II," JOURNAL OF FLUID MECH., Vol 27, pp 417-444, 1967.

15. Gargett, A. E., Hughes, B. A., "On the Interaction of Surface and Internal Waves," JOURNAL OF FLUID MECH., Vol 52, P. 1, pp 179-191, 1972.

16. Longuet-Higgins, M. S., Stewart, R. W., "The Changes in Amplitude of Short Gravity Waves on Steady Nonuniform Currents," JOURNAL OF FLUID MECH., Vol 10, p 4, pp 565-583, 1961.

17. Longuet-Higgins, M. S., Stewart, R. W., "Changes in the Form of Short Gravity Waves and Tidal Currents," JOURNAL OF FLUID MECH., Vol 8, P 4, pp 529-549, 1960.

18. Lewis, J. E., Lake, B. M., Ko, D.R.S., "On the Interaction of Internal Waves and Surface Gravity Waves," JOURNAL OF FLUID MECH., Vol 63, P 4, pp 773-800, 1974.

[351-5303]

5303
CSO: 1865

UDC 551.46.083

CHARACTERISTICS OF REMOTE SOUNDING INSTRUMENTS IN THE PRESENCE OF INTRINSIC NOISE

Sevastopol' MORSKIYE GIDROFIZICHESKIYE ISSLEDOVANIYA in Russian No 3, 1979 pp 142-150

[Article by M. G. Poplavskaya]

Abstract: The article gives an analysis of the characteristics of instruments for remote sounding of the ocean surface: gain in measurement accuracy, change in signal-to-noise ratio and transmission band, obtained as a result of optimum correction of the signals of these instruments. It is shown that optimum correction considerably improves the metrological characteristics of remote instruments.

[Text] One of the most important problems in measuring physical fields at the ocean surface by remote instruments installed on flightcraft is an increase in their resolution. Methods are now known which make possible instrumental solution of this problem. For example, the authors of [1] proposed a method based on use of coherent optical apparatus for the processing of data obtained using side-looking radar with a synthesized aperture. However, this method is unsuitable when processing the signals of a passive radar. The authors of [2] presented a mathematical method for increasing the resolution of remote sounding instruments -- optimum linear correction of their output signals, whose objective is to bring the shape of the corrected signal closer to the shape of the measured process, observed at the center of a resolution element. It examines an ideal case when the internal noise of the instruments is not taken into account. Allowance for the influence of the internal fluctuation noise of the instruments seriously limits the possibilities of the correction itself.

In this article we examine the increase in resolution of remote instruments by the method of optimum correction of their output signals, taking internal noise into account. The theoretical aspects of solution of this problem were presented in [3]. It describes a method for correction applicable to an additive mixture of signal and internal noise of the

instrument (the noise is assumed to be "white" and uncorrelated with the signal), first transmitted through an RC filter. Expressions were derived for the spectrum of the instrument correction function and the gain in measurement accuracy on the assumption of homogeneity, isotropicity and a "frozen-in" character of the field. As an application of the results we used theoretical models of the field and the instrument function for an instrument whose spectra had the form of a Gaussian curve. The advantage of such models is the possibility of representing the investigated characteristics in simple analytical form.

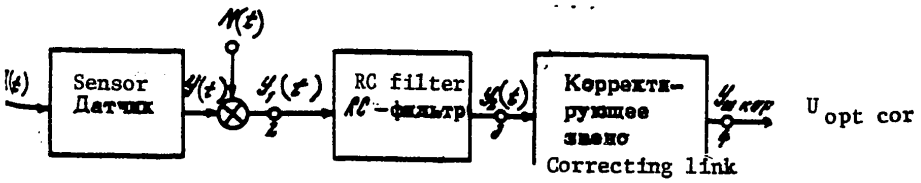

Fig. 1. Equivalent circuit of remote sounding instrument.

KEY:
A) Sensor
B) RC-filter
C) Correcting link

In this article we give an analysis of the gain in measurement accuracy, change in the signal-to-noise ratio and the transmission band as a result of optimum correction for models of fields whose one-dimensional spectrum has the form [4]

$$G_1(\alpha) = \sigma^2 \frac{\Gamma(p+1/2)}{\sqrt{\pi}\,\Gamma(p)} \frac{\beta^{2p}}{(\beta^2+\alpha^2)^{p+1/2}}, \qquad (1)$$

where 2 p + 1 is the degree of decrease of the spectrum with an increase in frequency. We examined remote instruments with sensors of four types:
1) sensor with uniform averaging;
2) sensor with the instrument function $x^{1/3} K_{1/3}(x)$ ($K_\nu(x)$ is the Macdonald function);
3) sensor or the radiometer carried aboard the "Cosmos-149" satellite [5];
4) sensor of the wide-angle radiometer used in making measurements from the TIROS-II satellite [6].

The spatial-spectral characteristics of these sensors were investigated in [7].

Figure 1 shows the equivalent circuit of a remote sounding instrument. Here X(t) is the input signal; Y(t) is the signal at the sensor output; N(t) is instrument internal noise; $Y_1(t)$ is the signal and noise mixture; $Y_2(t)$ is

the signal at the output of the RC filter; $Y_{opt\ cor}$ is the signal after optimum correction.

The measure of the gain in accuracy of measurement with optimum correction, in accordance with [3], is

$$\mu = \sigma_2^2/\sigma^2_{cor\ min},$$

where

$$\sigma_2^2 = \overline{\left[Y_2(t) - X(t)\right]^2},$$

and

$$\sigma^2_{cor\ min} = \overline{\left[Y_{opt\ cor}(t) - X(t)\right]^2}$$

One of the quality criteria for the mesuring system is the signal-to-noise ratio. By this term is meant the ratio of signal power to noise power. The greater this ratio, the higher is the quality of field measurement. Assume that η_1 is the signal-to-noise ratio at the RC filter output (point 3, Fig. 1) and η_2 is this ratio after signal correction (point 4, Fig. 1). Then the $\eta = \eta_2/\eta_1$ value characterizes the change in the signal-to-noise ratio as a result of correction and

$$\eta_1 = \frac{\int_0^\infty C(\omega)\left|\tilde{P}(\omega)\right|^2 d\omega}{\int_0^\infty S(\omega)\left|\tilde{P}(\omega)\right|^2 d\omega}, \tag{2a}$$

$$\eta_2 = \frac{\int_0^\infty C(\omega) A_1^2(\omega)\, d\omega}{\int_0^\infty S(\omega) A_1^2(\omega)\, d\omega}, \tag{2b}$$

and in turn

$$A_1(\omega) = \tilde{P}(\omega)\cdot\tilde{U}(\omega) = \frac{A(\omega)}{C(\omega)+S(\omega)}.$$

Here $C(\omega)$ is the energy spectrum of the signal at the instrument sensor input; $A(\omega)$ is the reciprocal energy spectrum of the signal at the sensor output and the field at the center of its resolution element; $S(\omega)$ is the noise energy spectrum N(t); $\tilde{P}(\omega)$ is the frequency characteristic of the RC filter. The function

$$\tilde{U}(\omega) = \frac{A(\omega)}{\tilde{P}(\omega)\left[C(\omega)+S(\omega)\right]} \tag{3}$$

is the frequency characteristic of the optimum correction of the instrument signal with its fluctuation noise taken into account.

We will find the $\mathcal{H}$ value characterizing the change in the transmission band of the corrected instrument. We will denote the spectral characteristics of the instrument before and after correction by $K_1(\omega)$ and $K_2(\omega)$ respectively. Taking into account that the spectral characteristic of the instrument is [7] the ratio of the signal energy spectrum to the noted one-dimensional energy spectrum of the field $Q_1(\omega)$ (here the instrument noise is not taken into account) we find that the signal power transfer coefficient from point 1 to point 3 (Fig. 1) is

$$K_1(\omega) = \frac{C(\omega)}{Q_1(\omega)} \left|\tilde{A}(\omega)\right|^2, \tag{4}$$

and this coefficient from point 1 to point 4 is

$$K_2(\omega) = K_1(\omega) \left|\tilde{U}(\omega)\right|^2. \tag{5}$$

Denoting by ω_1 and ω_2 the frequencies satisfying the ratios

$$K_1(\omega_1) = 0{,}5, \qquad K_2(\omega_2) = 0{,}5,$$

we find that the presence of a correcting link increases the instrument transmission band by a factor of $\mathcal{H} = \omega_2/\omega_1$.

The complex program prepared for an M-220M electronic computer makes it possible using the initial mass of data, describing any instrument function with axial symmetry, to compute the parameters μ, η and $\mathcal{H}$ with different $z = R_x/L_x$ values (except for $z = 0$, where an uncertainty arises); here R_x is the radius of a sensor resolution element; L_x is the characteristic scale of the measured field. The results of computations for different $S_1 = S(0)/C(0)$ values (where $S(0)$ and $C(0)$ are the energy spectra at zero for noise and signal respectively at the sensor output) are represented in figures and tables. The μ, η and $\mathcal{H}$ values with $z = 0$ for the value $P = 0.5$ were computed using the formulas

$$\mu = \frac{1 - \frac{1}{1+\gamma} + \frac{S_1}{\gamma}}{1 - \frac{1}{1+S_1} \cdot \frac{1}{1+\sqrt{\ell}}}, \quad \eta = 1{,}5\frac{\ell^2}{\gamma}\frac{F(2, 1/2; 3; 1-\ell)}{F(1, 1/2; 2; 1-\gamma^2)}, \quad z = \gamma\sqrt{\frac{\sqrt{2}-1}{S_1}}$$

where T is the time constant of the RC filter; $\gamma = V_0T/L_x$; $\ell = S_1/1 + S_1$; $F(\alpha, \beta; \gamma; t)$ is a hypergeometric function; V_0 is the velocity of instrument movement. For p different from 0.5 the μ, η and $\mathcal{H}$ values were computed approximately.

We will investigate the behavior of the μ, η and $\mathcal{H}$ curves in dependence on z for the considered sensors and field given by formula (1) with different p, γ and S_1 values in four cases: 1) different sensors with p, γ and S_1 equal to 0.5, 0.05 and 10^{-2} respectively; 2) the sensor of a SA radiometer with a change in the time constant of the RC filter ($\gamma = 0.05$; 0.25;

0.5) with p = 0.5 and $S_1 = 10^{-2}$; 3) sensor of a SA radiometer with constant p and γ values (p = 0.5 and γ=0.05) for different noise: $S_1 = 10^{-4}$ (low noise) and $S_1 = 10^{-2}$ (considerable noise); 4) sensor of a SA radiometer with S_1 and γ constant, equal to 10^{-2} and 0.05 respectively for P = 0.5 and 1.

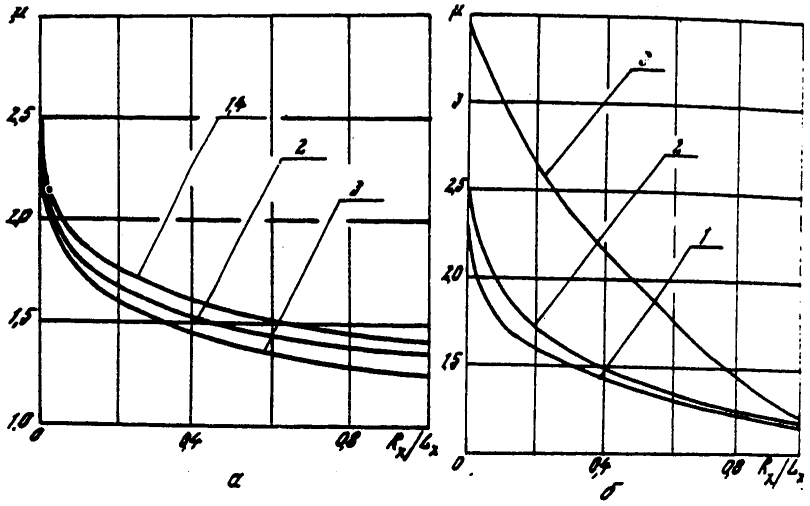

Fig. 2. Dependence of gain in measurement accuracy on z value: a) for sensors: 1) with uniform averaging; 2) with instrument function $x^{1/3} K_{1/3}(x)$; 3) "Cosmos-149"; 4) TIROS-II wide-angle radiometer; b) for radiometer of "Cosmos-149" satellite (SA): 1) γ = 0.05; 2) γ = 0.25; 3) γ = 0.5.

The effectiveness of optimum correction is determined by the value $\mu \geq 1$; the greater the μ value, the more effective is the correction. We will examine the change in this value in dependence on the variable z for the cases considered above.

In the first case (Fig. 2,a) all the μ curves decrease with an increase in z (with an increase in the radius of a resolution element) first rapidly, for $0 \leqslant z \leqslant 0.1$, and then more slowly, remaining greater than 1. The maximum μ value is attained with z = 0 ($\mu \approx 2.5$). Curves 1 and 4 merge into one. By comparing the gain in measurement accuracy for different sensors we find that they are quite close to one another.

By analyzing the gain $\mu(z)$ in the example of the SA radiometer sensor we note that it increases with an increase in the γ value (with an increase in the time constant T of the RC filter). In particular, for z = 0.1 and γ = 0.05 μ= 1.72, but with γ = 0.5 the gain is equal to 3.03 (Fig. 2,b). This is attributable to the fact that with an increase in the time constant of the RC filter the error at its output, according to [3], increases

considerably more rapidly than the error obtained after correction.

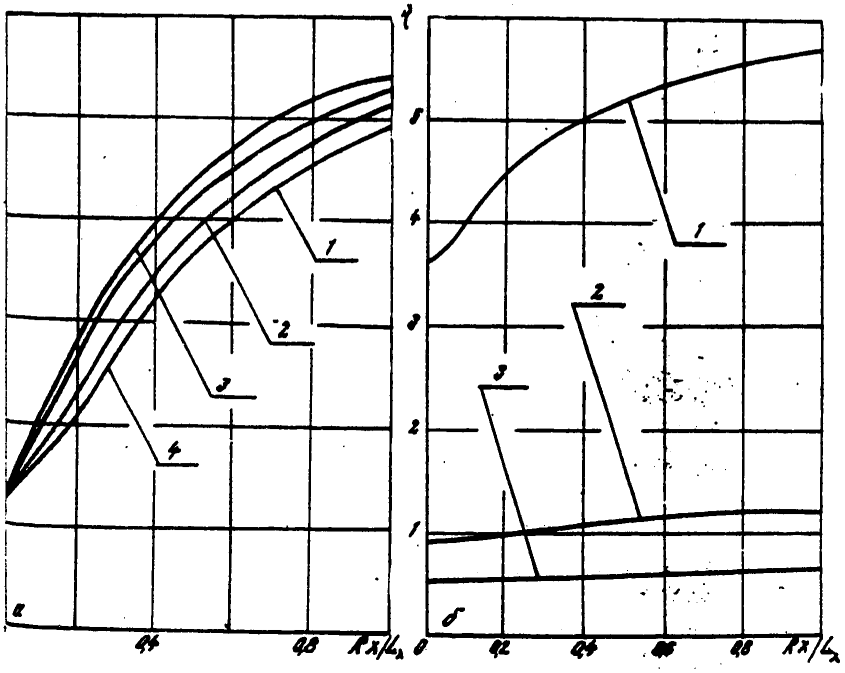

Fig. 3. Dependence of signal-to-noise ratio on z.

An increase in noise (case 3, δ = 0.05 and p = 0.5) decreases the gain, which is especially conspicuous in the case of small z values. Whereas for z = 0.01 and $S_1 = 10^{-4}$ μ = 2.70, with $S_1 = 10^{-2}$ the μ value is equal to 2.10. This occurs because with an increase in noise the correction error increases more rapidly than with filtering.

We carried out a comparison for analysis of the gain in measurement accuracy for fields with different degrees of decrease in the spectrum (fourth case). It was established that high values (spectra that drop off more steeply) correspond to high gain values, especially for z close to zero. For example, with z = 0 in the case p = 1/3 μ = 2.2, whereas with p = 5 the gain is equal to 3.4. Accordingly, the correction of physical fields with spectra that drop off more steeply is most effective.

In generalizing these results we note that the application of optimum correction to a mixture of signal and noise passed through an RC filter increases the measurement accuracy to a considerable degree in those cases when the radius of a resolution element is considerably less than the

characteristic field scale.

As indicated by computations, the optimum correction of signals of remote instruments not only decreases the measurement error, but in many cases increases the signal-to-noise ratio. We will investigate how this ratio behaves in the considered four cases. Figure 3,a shows that the signal-to-noise ratio everywhere exceeds unity and increases with an increase in the z value (the notations are the same as in Fig. 2).

In the second case (Fig. 3,b) with an increase in the time constant of the RC filter there is a decrease in the η ratio. It is characteristic that in the region of small z values with $\gamma = 0.25$, and also for all $0 \leqslant z \leqslant 1$ with $\gamma = 0.5$ η is less than 1. This occurs because with an increase in the time constant of the RC filter the signal-to-noise ratio as a result of filtering increases, at the same time that this constant exerts no influence on the correction; this follows from formula (2). For $\gamma = 0.05$ $n \gg 1$ everywhere and increases with an increase in z.

Comparing the η value for different noise values (third case) we find that it is less than 1 for all $0 \leqslant z \leqslant 1$ for small noise; with an increase in z the η value decreases, but in the case of considerable noise η is an increasing value, exceeding 1. For example, $\eta = 3.65$ with $z = 0$ and $S_1 = 10^{-2}$. It therefore follows that with optimum correction an increase in noise also results in an increase in the signal-to-noise ratio.

As indicated by computations in the fourth case, the signal-to-noise ratio increases with an increase in the steepness of the field spectrum. Whereas $\eta = 4.06$ with $z = 0.1$ and $p = 0.5$, with $p = 1$ the η value is equal to 5.28. With an increase in z the value of the signal-to-noise ratio increases. The optimum correction gives a greater effect for steeper field spectra both in a gain in measurement accuracy and in the value of the signal-to-noise ratio.

Thus, as a result of correction in the case of considerable noise, and also for steeper field spectra and a small time constant of the RC filter, for all $0 \leqslant z \leqslant 1$ values η considerably exceeds unity.

We will investigate the change of the transmission band for the 0.5 level of the corrected signal, assuming that the signal (without allowance for noise) is transmitted through the RC filter and is subjected to correction. Since the spectrum of the optimum correction instrument function, as follows from formula (3), is dependent on noise, the latter will be reflected in the $\mathcal{H}$ value. An analysis indicated that in the first case for all sensors $\mathcal{H}$ is less than 1 in the region of small z values, that is, when $R_x \ll L_x$ there is a narrowing of the transmission band of the corrected signal.

With an increase in the time constant of the RC filter (Table 1) the transmission band becomes wider. For example, with $z = 0.1$ for $\gamma = 0.05$ it is equal to 0.78, whereas with $\gamma = 0.25$ the value $\mathcal{H}$ is equal to 1.61 and

with γ = 0.5 assumes a value 2.57. This is attributable to the fact that with an increase in T, in accordance with formula (4), there is a narrowing of the transmission band after filtering, whereas in the case of correction it does not change. As a result, the instrument transmission band after correction is broadened.

Table 1

Transmission Band of Signal of Corrected Instrument as a Function of z for Different γ Values

γ \ z	0	0,01	0,1	0,3	0,5	0,7	1
0,05	0,318	0,341	0,783	1,081	1,430	1,800	2,020
0,25	1,550	1,590	1,650	1,710	1,820	1,882	2,201
0,50	3,200	3,009	2,601	2,420	2,331	2,260	2,200

Table 2

Transmission Band of Signal of Corrected Instrument as a Function of z for Different Noise

δ_η \ z	0	0,01	0,1	0,3	0,5	0,7	1
10^{-4}	3,200	3,250	3,350	3,440	3,542	3,620	3,700
10^{-2}	0,318	0,341	0,783	1,081	1,430	1,800	2,020

It follows from the data in Table 2 that a decrease in noise leads to an increase in the $\mathcal{H}$ value. Since noise exerts no influence on filtration and its decrease leads to an improvement in the correction result, as a result there is a broadening of the transmission band. In the case of very small z the broadening is insignificant; with their increase it increases and already when z = 0.1 attains values $\mathcal{H}$ = 2.19. For fields with a rapidly decreasing spectrum (fourth case) the transmission band is narrowed and in the region R_x, small in comparison with L_x, the values $\mathcal{H} < 1$.

Summary

1. Optimum correction always gives a gain in measurement accuracy; it increases with a decrease in the radius of a resolution element.

2. With optimum correction there is the greatest increase in the signal-to-noise ratio for fields with a steeper spectrum and also with considerable noise and a small value of the time constant of the RC filter.

3. An increase in the time constant of the RC filter and a decrease in noise leads to a broadening of the transmission band of the corrected signal.

BIBLIOGRAPHY

1. Katron, L. Dz., et al., "Application of Coherent Optical Methods for the Processing of Signals in Radar Apparatus With a Synthetic Aperture," TRUDY INSTITUTA INZHENEROV PO ELEKTROTEKHNIKE I RADIOELEKTRONIKE (Transactions of the Institute of Electrical and Radioelectronic Engineers), Vol 54, No 8, Moscow, pp 11-19, 1966.

2. Nelepo, B. A., Dotsenko, S. V., Poplavskaya, M. G., "Optimum Field Restoration Using the Results of Remote Sounding," MORSKIYE GIDROFIZICHESKIYE ISSLEDOVANIYA (Marine Hydrophysical Research), No 1, Sevastopol', pp 40-55, 1976.

3. Dotsenko, S. V., Nelepo, B. A., Poplavskaya, M. G., "Optimum Correction of Signals of Remote Instruments With Allowance for Their Internal Noise," MORSKIYE GIDROFIZICHESKIYE ISSLEDOVANIYA, No 1, Sevastopol', pp 125-128, 1977.

4. Monin, A. S., Yaglom, A. M., STATISTICHESKAYA GIDROMEKHANIKA (Statistical Hydromechanics), Part 2, Moscow, "Nauka," 1967, 720 pages.

5. Gorodetskiy, A. K., et al., "Method and Some Results of Determination of the Underlying Surface from the 'Cosmos-149' Satellite," IZV. AN SSSR, FAO (News of the USSR Academy of Sciences, Physics of the Atmosphere and Ocean), Vol 5, No 4, pp 355-367, 1969.

6. Astkheymer, R., de Vaard, R., Dzhekson, Ye., "IR Radiometers on the TIROS-II Satellite," RAKETY I ISKUSSTVENNYYE SPUTNIKI V METEOROLOGII (Rockets and Artificial Satellites in Meteorology), Moscow, IL, pp 158-170, 1963.

7. Dotsenko, S. V., Nedovesov, A. N., Poplavskaya, M. G., Ryzhenko, V. A., "Spatial-Spectral Characteristics of Remote Sensors," MORSKIYE GIDROFIZICHESKIYE ISSLEDOVANIYA, No 2, Sevastopol', pp 162-173, 1974.

[351-5303]

5303
CSO: 1865

UDC 629.12:621.396

CHOICE OF TRANSMITTING ANTENNAS AND WORKING FREQUENCIES FOR A RADIO CHANNEL FOR SEA BUOYS

Sevastopol' MORSKIYE GIDROFIZICHESKIYE ISSLEDOVANIYA in Russian No 3, 1979 pp 151-155

[Article by V. S. Nazarov and M. N. Pen'kov]

Abstract: The article briefly sets forth a comparative evaluation of several types of transmitting antennas and recommendations on their installation on sea buoys and on determination of the optimum working frequency of the antenna.

[Text] In modern investigations of the seas and oceans extensive use is made of anchored or drifting buoy stations outfitted with instruments for measuring hydrophysical and meteorological parameters. The routine transmission of data from stations to the point of collection of information, situated aboard a ship or on shore, is through a radio channel, for which radio transmitters and antennas are situated at the station. Depending on the formulated physical problem and the necessary communication range, appropriate requirements are imposed on the radio channel with respect to the rate of data transmission, type of modulation, power, frequency, etc. These factors, together with allowance for the design peculiarities and possibilities of buoy buoyancy to a large extent are decisive in choosing the type and design of the transmitting antenna. Its directional diagram in a general case must be must be circular in the horizontal plane and the polarization must be vertical, since the antenna is situated in the immediate neighborhood of the sea surface.

In order to ensure stable communication, increase the signal-to-noise ratio at the reception point and for effective use of transmitter power it is necessary that the efficiency of the antenna circuit insofar as possible approach unity. The latter is determined by the ratio of useful radiation resistance and resistance to antenna circuit losses. The losses in turn are dependent on the rigging and superstructures situated alongside, on buoyancy, on grounding (sea water) resistance and on the quality of the element for tuning the antenna circuit to resonance. The first two

conditions are rigidly stipulated and cannot be changed. The quality of the tuning element (extended inductance coil for electrically short antennas) must be made as large as possible in order to reduce the resistance to losses in it and thereby increase the efficiency. Finally, in order to increase efficiency the antenna must have geometric dimensions commensurable with the length of the working wave. For small buoy installaations this cannot be accomplished in the range of short waves but is not difficult in the ultrashort-wave range, using a quarter-wave or half-wave vibrator as the transmitting antenna.

With distances between the reception point and buoy not exceeding the range of direct visibility (20-25 km) the use of the ultrashort-wave range for communication is preferable from the design and electric point of view. However, beyond this distance the field strength rapidly decreases and reception becomes impossible. In this case stable communication at any time of day with an extent of the radio link of several tens and hundreds of kilometers can be accomplished on short, medium and long waves having a high capacity for bending around the earth's surface (see the field strength curves of the International Consultative Committee on Radio Communications for propagation over the sea [1, 2]).

The limitation of space on buoys with a displacement up to several tons does not make it possible to place antennas with large linear dimensions on them. Light and small antennas, such as loop antennas with a loop area of 1-2 m^2 and ferrite antennas at SW frequencies have a small radiation resistance and a very low efficiency of about 10^{-3} [3]. In addition, the tuning of a ferrite transmitting antenna in strong electromagnetic fields is dependent on the power conducted to it, and accordingly, is unstable. But under definite conditions, in low-power transmitters, this antenna may be preferable to others. In comparison with a short type of electric antenna, for a ferrite antenna the dependence of tuning on the immediate surroundings is expressed much more weakly. If both antennas of equal effective height are submerged in sea water the density of the field emitted by the magnetic antenna will be greater than for the electric antenna by 11 db, which is attributable to the better conditions for matching of the magnetic antenna. With the positioning of both emitters in the immediate neighborhood of the conducting medium (for example, sea water), the conditions for the propagation of radio waves emitted by the magnetic antenna will be more favorable. This increases the effective range of the latter if the power emitted by both antennas is identical. The use of magnetic antennas for communication for hundreds of kilometers is undesirable and on the buoys it is necessary to use a linear vertical vibrator whose length may be several meters, depending on construction-design possibilities.

The effectiveness of an antenna of stipulated dimensions and parameters must be evaluated on the basis of the field strength which it creates at a stipulated distance and the frequency at the reception point. With an increase in the working frequency the power emitted by the electrically

short antenna and its efficiency increases. Beyond the limits of direct visibility the field strength of the surface wave decreases more rapidly for the higher frequencies than for the low frequencies. Accordingly, there is an optimum value of the working frequency of the antenna at which there is assurance of a maximum field strength at a stipulated distance in the diffraction zone, all other conditions being equal.

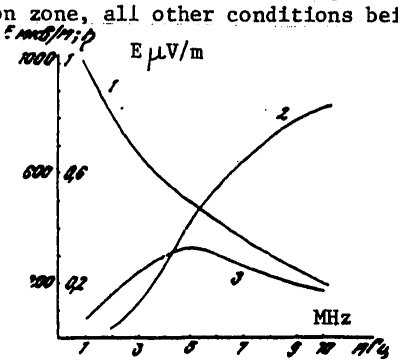

Fig. 1. Curve of the dependence of field strength and antenna efficiency on frequency.

Figure 1 shows curves of the dependence of field strength E on frequency at a distance of 200 km from a vertical emitting vibrator with a transmitter power p = 1 KW and with propagation over the sea surface. Curve 1 was constructed using the International Consultative Committee on Radio Communication curves for 1 KW emitted power, that is, without efficiency taken into account [1, 2]. Curve 2 represents the change in antenna efficiency as a function of frequency; the antenna used was a collapsible-whip antenna with a length of 6 m; the quality of the induction coil was 100. The loss resistance at the base of the antenna was determined using the formula

$$R_{\text{пр}} = A\frac{\lambda}{\lambda_0} + B\frac{\lambda_0}{\sqrt{\lambda}} \quad \text{ohm},$$

where it was assumed that A = 0.35, B = 0.3 [4].

On the basis of the known radiation resistance of the vibrator and the determined values of the total loss resistance we computed the efficiency of the antenna circuit for a number of frequencies (curve 2); then we determined the resulting field strength (curve 3).

$$E_1 = E\sqrt{\eta},$$

where E are the corresponding values of the curve 1; η is the efficiency of the antenna circuit.

It can be seen that E_1 with an increase in frequency and efficiency first increases, attains a maximum, and then decreases, tending to the values of the curve 1. The frequency corresponding to the maximum of the curve 3

is optimum for the particular antenna and distance. With a communication range greater than 200 km the maximum of curve 3 is displaced in the direction of the lower frequency, decreasing in absolute value, but with lesser distances is displaced in the direction of the high frequencies and increases. With extents of the radio path greater than 400 km in the computations it is necessary to take into account the spatial component of the wave, especially at nighttime.

Thus, in order to find the optimum working frequency for the buoy radio transmitter it is necessary to know the parameters of the antenna and the distance to the reception point, which are determined taking into account the formulated problem and design possibilities. Then, using the method cited above, a graph is constructed and the frequency of the maximum of curve 3 or a frequency close to it is selected.

A collapsible-whip antenna with lower current supply and an Ayzenberg antenna with a capacitance load and upper current supply, whose base was grounded, will be admissible for installation on buoys. Both antennas have vertical polarization and a circular directional diagram in the horizontal plane. However, the effective height of the antenna with upper current supply and its radiation resistance is higher than for a collapsible-whip antenna.

As a comparison, the table gives the computed values of efficiency of antennas of both types of equal geometric lengths 4 and 6 m at a frequency of 3.7 MHz. The loss resistances at the antenna bases (across the terminals) were assumed to be identical. The quality of the tuning induction coils was assumed to be 100; the diameter of the capacitance load umbrella was 2 m.

Table 1

Antenna type	Length, m	Tuning inductance, μg	Coil loss resistance, ohm	Loss resistance at base, ohm	Radiation resistance ohm	Efficiency
With upper current supply of 2-m umbrella	4	13.05	2.95	1.9	4	0.45
	6	11.46	2.52	1.8	9	0.67
Collapsible-whip	4	41.3	9.94	1.9	0.95	0.08
	6	31.7	7.17	1.8	2.05	0.19

The table shows that the efficiency of an antenna with upper current supply is several times greater than for a collapsible-whip antenna of the same length. The gain is attributable both to the higher radiation resistance of the first antenna and the lesser tuning inductance because of the capacitance of the umbrella, and accordingly, the lesser losses in the coil. If the umbrella capacitance is made such that the tuning coil of both antennas is identical, in this case the efficiency of the first antenna will be approximately twice greater than for the second. In order to obtain a signal of the same intensity from the collapsible-whip antenna as from the umbrella antenna, it is necessary to increase the transmitter power by a corresponding number of times. This results in a complication of its design, and also an increase in the volume of the current sources or a decrease in the autonomy of the buoy complex, and this may be unacceptable. Under stormy conditions the low-placed input terminal and part of the collapsible-whip antenna will be immersed in water. If the transmitter is switched on under such conditions there will be a marked change in the load, to all intents and purposes a short-circuiting for the high frequency and possibly transmitter failure. In order to prevent damage to the circuit it is necessary to introduce a protection device, which still further complicates transmitter design. In the Ayzenberg antenna the input terminals are situated in the upper part of the mast and the washing of its base by a wave during the time of operation is of no great danger, causing only some decrease in its effective height and virtually not changing the tuning of the antenna circuit to the working frequency. In addition, different kinds of instrumentation can be placed on the grounded mast: navigational lights, measuring sensors, etc., with current supply to the cable network from below. However, with respect to design the collapsible-whip antenna is less complex and unwieldy.

Thus, for the transmission of information from an autonomous sea buoy for a distance up to hundreds of kilometers preference must be given to an antenna with an upper current supply, having overall better electric and operational characteristics. It is necessary to find the optimum working frequency from the known distance and parameters of the antenna circuit. Ultrashort wave antennas and magnetic antennas can be preferable to others at short distances and under specific conditions.

BIBLIOGRAPHY

1. Dolukhanov, M. P., RASPROSTRANENIYE RADIOVOLN (Radio Wave Propagation), Moscow, "Svyaz'," pp 56-128, 1965.

2. Tarnetskiy, A. A., Osipov, D. D., ANTENNY SUDOVOY RADIOSVYAZI (Antennas for Ship Radio Communication), pp 18-24, Leningrad, Sudpromgiz, 1960.

3. Khomich, V. I., FERRITOVYYE ANTENNY (Ferrite Antennas), Moscow, "Energiya," pp 55-62, 1969.

4. Vershkov, M. V., SUDOVYYE ANTENNY (Shipboard Antennas), Leningrad, "Sudostroyeniye," 1972, 320 pages.

[351-5303]

5303
CSO: 1865

UDC 551.46.084

COMPLEX METHOD FOR MEASURING THE FIELD OF GAMMA RADIATION OF SEA WATER

Sevastopol' MORSKIYE GIDROFIZICHESKIYE ISSLEDOVANIYA in Russian No 3, 1979 pp 156-169

[Article by I. F. Lukashin, V. N. Yeremeyev, G. F. Batrakov, A. M. Vinnikov and A. V. Kukharchik]

Abstract: The article describes the principle for simultaneous registry of the cascade and total γ-background, as well as its anisotropy, in the case of in situ measurements. Data are cited for computing instrument geometry, on the basis of which it was possible to construct a model of a three-channel γ-complex. The informative parameters of the instrument are investigated. The stages in processing of statistical information are given.

[Text] In connection with the continuing intensive contamination of the world ocean with the wastes of atomic industry enterprises, in a number of countries of the world work is continuing on the creation and improvement of instrumentation for a direct method of in situ registry of radioactivity of sea water [1-9].

In order to detect correlations between the types and characteristics of the environment, on the one hand, and the parameters of their remote manifestations, on the other, it is customary to carry out measurements and a theoretical analysis of cause-and-effect relationships between different aspects of phenomena transpiring in the medium. The indicators of natural formations are established on the basis of spectral, spatial and evolutionary characteristics. Measurements of radioactivity of the water medium -- identification and determination of the components (usually a great number) of the radioactive background in this respect have a number of specific peculiarities of sea water.

Due to the fact that the activities of the isotopes of interest to the researchers are usually small and are at the limit of response of the method use is made of instrumental solutions for discriminating emission of the isotope from the general γ-background of sea water. For the most part this has been energy differentiation of radiation incident in the detector -- spectrometry.

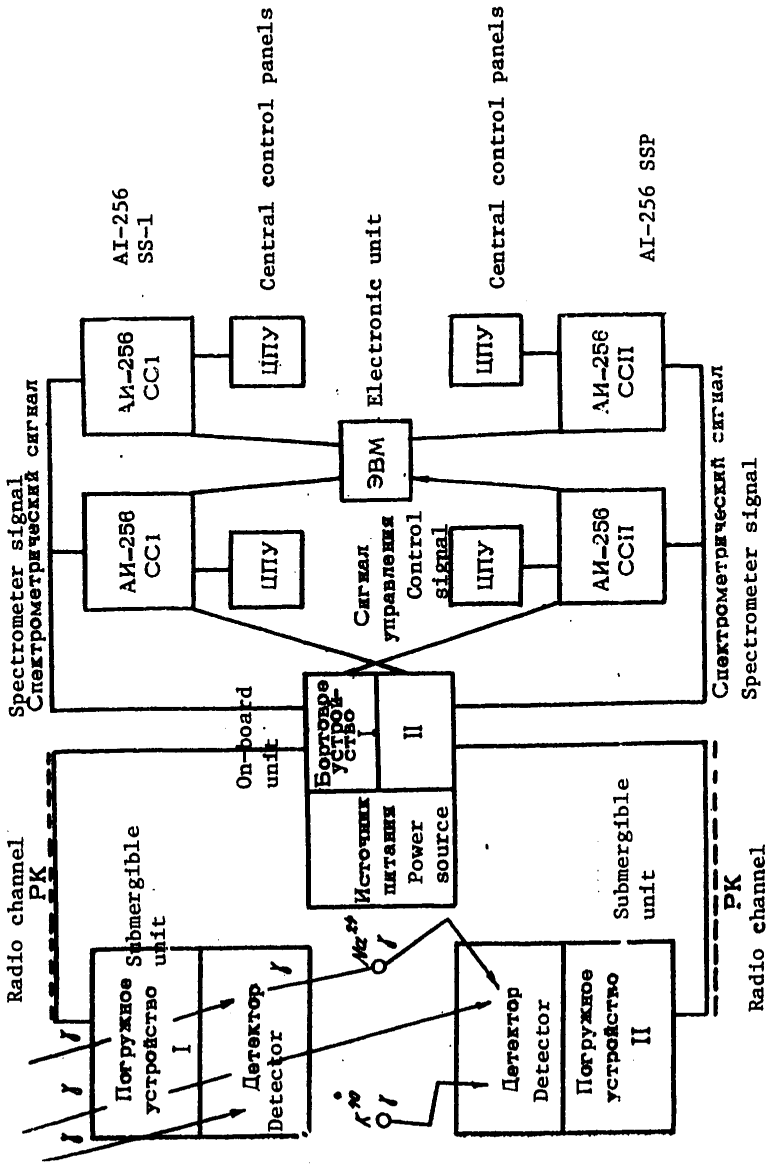

Fig. 1. Block-diagram of two-channel instrument complex.

The principal shortcomings of the instrument complexes created for this purpose [1-9] are a long exposure time due to the low efficiency of the radiation detectors, low identification capability, considerable temporal instability of the electronic instrumentation of the submergible unit, and high characteristic background of the instrumentation in comparison with fluctuations of the natural background of sea water.

The registered γ-background of sea water consists of the radiation of radionuclides of natural and artificial origin, the background of cosmic radiation, characteristic background of the instrument, including the characteristic background of the detectors and different kinds of errors in electronic circuits.

This article describes a method for separation (rejection) of the last two components of the γ-background of sea water for studying the structure of variations of the first. It is solved on the basis of the principle of fast γ-spectrometry of radiation of the medium by a multichannel instrument with independent and identical channels, rational choice of instrument geometry and statistical processing of the maximum volume of spectrometric information using an electronic computer.

The principle of instrument operation is clarified in Fig. 1, which shows a two-channel γ-complex, making it possible to differentiate the radiation applying the principles of spectrometry of total γ-radiation (energy differentiation), spatial anisotropy and spectrometry of cascade γ-radiation ("time" rejection).

The construction and use of such measurement systems requires a knowledge of the effectiveness of the detectors, the registered flux of γ-radiation and the effective emitting volume of the medium.

As done by the authors of [16], we will replace the usually used cylindrical NaI(Tl) crystal by a spherical detector of the radius R of equal volume. [Here and in the text which follows the unit of measurement of linear dimensions is $1/\mu$; μ is the linear coefficient of attenuation of radiation in the medium.] Then, in accordance with [6], the expression for the flux of γ-radiation in the detector from the spherical layer Δr, at the distance r from the center of the detector, has the form

$$\Delta\Phi(r)=\frac{\pi A}{\mu^3}\int_R^{r+R}\alpha'\xi'\cdot\xi'\int_{\xi'-R}^{\sqrt{\xi'^2-R^2}}e^{-\xi'\left(\xi'^2\rho^{-2}-R^2\rho^{-2}-1\right)}d\rho, \qquad (1)$$

A is medium activity; ξ' and ρ are integration variables. Introducing the values

$$\alpha=R\sqrt{\left(\frac{r}{R}\right)^2-1} \quad \text{and} \quad \beta=R\left(\frac{r}{R}-1\right)$$

and taking into account that

$$\varepsilon_n(x)=\int_1^{\infty}e^{-xu}u^{-n}du,$$

expression (1) is easily reduced to the form

$$\Delta\Phi(r) = \frac{2\pi A}{\mu^3}\, r\left[R\varepsilon_2(\beta) + \varepsilon_3(\alpha) - \varepsilon_3(\beta)\right]\Delta r. \qquad (2)$$

(Tables of the functions $\mathcal{E}_n(\chi)$ can be found, for example, in [7].)

The probability that a γ-quantum, generated at the distance r from the center of the detector, will enter its volume, from (2) is equal to

where

$$\Phi(r) = \frac{1}{2}\frac{1}{r}\psi(R,\alpha,\beta)\ ,$$

$$\psi(R,\alpha,\beta) = R\varepsilon_2(\beta) + \varepsilon_3(\alpha) - \varepsilon_3(\beta)\ . \qquad (3)$$

The total flux of unscattered radiation in the volume of the detector or in a cavity cut by the detector in the medium is obtained by integration of expression (2) for r in the limits R - r

$$\Phi(r) = \frac{\pi A}{\mu^3} R^2\left\{1 + \frac{r}{R^2}\left[\left(e^{-\beta} - e^{-\alpha}\right) - 3\left(\varepsilon_5(\beta) - \varepsilon_5(\alpha)\right)\right] - 2\frac{r}{R}\varepsilon_3(\beta)\right\}. \qquad (4)$$

At the limit with $r \to \infty$ the expression in the braces (4) becomes equal to unity and the total radiation flux in the cavity R assumes the form

$$\Phi(\infty) = A\pi R^2 \cdot \frac{1}{\mu^3}\ . \qquad (5)$$

Formula (5) for the first time was derived by Kosourov [8] by an independent method.

Within the discriminated cavity the field of γ-radiation is homogeneous and isotropic; therefore, the flux incident in the detector R_0, placed in the cavity R, is equal to

$$\Phi_0 = A\pi R^2 \frac{\pi R_0^2}{\pi R^2}\frac{1}{\mu^3} = A\pi R_0^2\frac{1}{\mu^3} \qquad (6)$$

and, as was noted by Vinogradov [4], is not dependent on the dimensions of the protective shell of the detector, that is, on the dimensions of the cavity. The effectiveness of the detector is determined using a formula proposed in [6],

$$\varepsilon = 1 - \left(1 - e^{-2\lambda}\right)(2\lambda)^{-1}\ , \qquad (7)$$

where

$$\lambda = \frac{\mu_0}{\mu} R_0 \gamma_0$$

is the linear coefficient of absorption of γ-radiation by the material of the detector.

The effective volume of the medium, emitting γ-quanta into the detector, is determined from expression (4). Figure 2 shows a graph of the dependence of the relative radiation flux (the expression in the braces in (4)),

intersecting the detector R, on the thickness of the emitting-absorbing layer of the medium (r - R) for different R. The relative flux is slightly dependent on the dimensions of the detector (by not greater than 10% for R in the range 0.1-2). A spherical layer with the thickness 0.5 gives a contribution to the total flux > 50%, with the thickness 1 -- ~ 75%, with the thickness 3 -- > 95%.

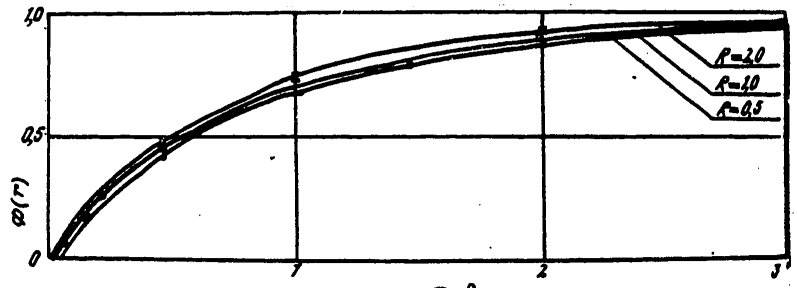

Fig. 2. $r-R$

Thus, the effective emitting volume of the medium for unscattered γ-radiation is limited to two or three lengths of the free path of a γ-quantum in the medium and is virtually not dependent on the dimensions of the detector. The periphery introduces a small contribution to the total radiation flux.

For computing the parameters of registry of cascade radiation by a system of two detectors R, placed in an isotropic emitting-absorbing medium at the distance 2ℓ from one another, we will use formula (3). For two cascade γ-quanta with an uncorrelated direction of escape the facts of their entry into one detector or the other are independent events. Accordingly, the probability of registry of a cascade generated at a point in space at the distances r and r' from the centers of the detectors is expressed by the dependence

$$\varphi_{jj}(r,r') = \frac{1}{r}\frac{1}{2}\frac{1}{r'}\psi(R,\alpha,\beta)\,\psi(R,\alpha',\beta'), \tag{8}$$

and the counting rate of the coincidences of cascade radiation in the active medium A is

$$\varphi_j = A\,\varepsilon_{jj}(r,r')\int_{\infty}\varphi_{jj}(r,r')\,dV. \tag{9}$$

The effectiveness of the cascade radiation detector is equal to

$$\varepsilon_{jj} = \varepsilon^2. \tag{10}$$

We carried out numerical computations of this dependence (8) (Fig. 3). We will represent expression (8) in Cartestian coordinates and we obtain

$$\varphi_{ij} = \left(\frac{Q}{\mu}\right) \pi^2 (\Delta S)^2 \left(\frac{j^2}{r r'}\right) \psi(\nu, x, z)\, \psi(\nu, x', z'),$$

$$r = \sqrt{j^2 + (\ell - i)^2}, \quad r' = \sqrt{j^2 + (\ell + i)^2},$$

$$x = \nu(\rho - 1), \quad x' = \nu(\rho' - 1),$$

$$z = \nu\sqrt{\rho^2 - 1}, \quad z' = \nu\sqrt{\rho'^2 - 1}, \qquad (11)$$

$$\rho = \sqrt{\left(\frac{j}{R}\right)^2 + \left(\frac{\ell}{R} - \frac{i}{R}\right)^2}, \quad \rho' = \sqrt{\left(\frac{j}{R}\right)^2 + \left(\frac{\ell}{R} + \frac{i}{R}\right)^2}, \quad \nu = \mu R,$$

where ΔS is an elementary area in the section of a system of detectors with a radial plane with the coordinates i and j.

In Cartesian coordinates the field of probability of registry of a cascade has a symmetry relative to the i-axis and the plane perpendicular to it which passes through the j-axis. Accordingly, computations are made in the first quarter of the plane for circular volumes with the section ΔS.

Figure 3 shows the results of the computations for $\mu R = 0.8$ and $\ell/R = 1.1$. The isolines represent lines of equal probability of registry of cascade radiation with an energy 1.3 MeV by sensors of the radius R. The values of the probability of registry of a cascade generated at a point in space are indicated in relative units in the numerator of the fraction. The greatest probability of registry relates to sources lying in the plane $j \perp i$ at the distance 0.4R from the center of the system, but due to an increase in the volume of the peripheral regions the flux of registered cascade radiation decreases slightly with distance from the center. This is indicated by the values of the integrals of probability of registry from the regions bounded by the isolines. In Fig. 3 they are given in the denominators of the fractions. The full integral for the space 10R is equal to 7719. Accordingly, the peripheral regions of space introduce a substantial contribution to the registered flux of cascade radiation.

In order to choose the optimum relationship of geometric dimensions of the detection system we carried out computations of the dependence of the integral of probability of registry of cascade radiation in space on the ratio ℓ/R, which was selected because specifically in such a combination the geometric parameters enter into expression (11).

Figure 4 gives the results of these computations, from which it follows that the maximum statistical probability of the measurement is with $\ell/R = 1$. However, due to the design peculiarities of the system and the conditions for its operation it is necessary that a part of the space with a maximum probability of registry be "cut out" by the sealed capsule of the detectors; this results in a considerable decrease in effectiveness of the system.

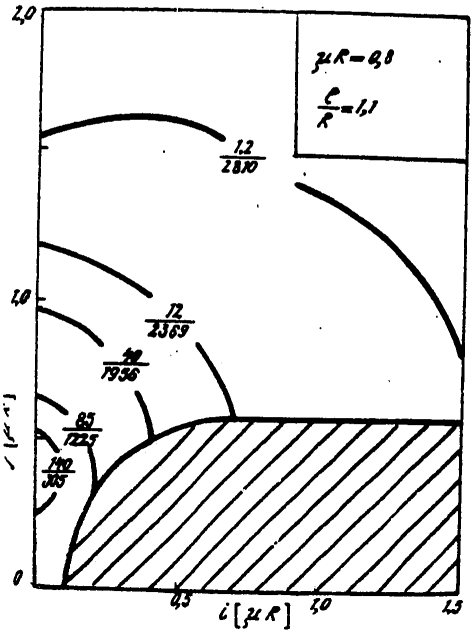

Fig. 3. Field of probability of registry of cascade radiation by a system of two detectors in a homogeneous emitting-absorbing medium.

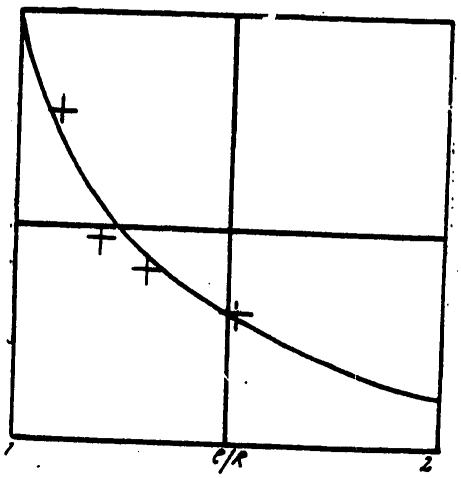

Fig. 4. Dependence of flux of cascade γ-radiation registered by γ - complex on distance between detectors. A) Integral of probability of registry.

The three-channel γ - complex used in investigating the radioactivity of sea water incorporates the above-mentioned merits of rejection of the background with a considerable increase in effectiveness, together with a low level of its own background. Its principal parameters are the following: weight -- 20 kg, dimensions $\varnothing$ 1200 x 500, limiting depth of submergence 100 m. The submergible part consists of three sealed capsules held in a rigid frame with a fixed distance between the BDEG2-6931-20 NaI(Tl) detectors $\varnothing$150 x 100, placed in them. The submergible unit also includes a highly stable system for electric supply of the detector and a communication line based on a cable of the RK type.

The intrinsic background of the sensors with respect to K^{40} emission (1.46 MeV) is 3-2 pulses$\cdot$min^{-1}; the effectiveness in the sea medium is not less than 20%. The on-board unit includes six AI-256-6 (two in each channel for registry of total and cascade γ -background), a unit for control of coincidence analyzers, and also a unit for the registry of information. Under field conditions the instrumentation indicated a high performance. The resolution of the spectrometric channels in the instrument was not

worse than 13% (in the Cs^{137} line -- 662 KeV), instability -- not greater than 1-2 channels in the 1.46-MeV line in 24 hours of continuous operation. Large detectors based on NaI(Tl) monocrystals with a working volume of 1.5 л or more are extensively used at the present time for γ-spectrometry and radiometry of small activities of natural media. The high effectiveness of the detector, in combination with great linear dimensions, makes it possible to accelerate analysis of the γ-field of radioactive elements of emitting-absorbing media. Due to the fact that the technology for the purification of NaI construction materials, glass, etc. from impurities of radioactive elements has not yet been developed to an adequate degree, the content of K^{40} isotopes and the members of the radioactive series in standard detectors is usually determined by the purity of the initial raw material and therefore is different even in articles of the same series.

We investigated three different types of NaI(Tl) detectors with crystals measuring: a) scintillation unit Ø150 x 100, BDEG2-6931-20, produced 1975; b) set of crystals Ø150 x 100 and a FEU-49 photomultiplier, produced in 1964; c) a set of NaI(Tl) crystals Ø 200 x 100 and a FEU-49 photomultiplier, produced in 1975 (Fig. 5), which we used for the γ-spectrometry of sea water. For discriminating the background of γ-radiation of radioactive origin in sea water we used the method of protection of the sensors by a layer of fresh water. For this purpose the set of γ-radiation sensors was placed in a rubberized cylinder with a volume of 5 m^3, fresh water was poured in the cylinder and it was sealed. Monitoring of the effectiveness of shielding against the radiation of the isotopes present in sea water was accomplished using the intensity of the K^{10} photopeak.

Normalized spectra of γ-radiation of sea water of different salinity 0, 17, 34°/oo for a depth of 60 m are shown in Fig. 5. In all the spectra, other than curve 1 (Fig. 5,a) there are intensive peaks of a natural γ-K^{40} radiation source; in measurements with a modern scintillation unit in fresh water this peak virtually disappears. In spectra obtained using an "a" detector in the soft energy range, due to the low intensity of the scattered radiation of high-energy sources, there are peaks of γ-radiation of the series U and Th, present in the construction materials of the detector; in others they are masked by intensive K^{40} scattered radiation. This is the peak 0.59 MeV, which must be attributed to the monolines 0.588, 0.511-Te^{208} (Th) and 0.609 - Bi^{214} (U), as well as the peak 0.92 of the monolines 0.911, 0964 and 0.969 MeV - Ac^{228} (Th). The intensities of these peaks are of the same order of magnitude due to the comparability of the content of U and Th in the construction materials of the sensors. In the spectra of series "a" there is also a series of less intensive peaks -- a result of superposing of the radiation of less intensive gamma lines of members of the U-Th series. These peaks are 0.35 MeV and 1.1-1.2 MeV.

In measurements at the water surface the intensity of these peaks (0.59 and 0.92 MeV) somewhat increases, in our opinion attributable to processes of inelastic interaction between cosmic radiation and the matter of the construction materials of the sensors, specifically: $Al^{27}(p, p', \gamma)$ Al^{27}; Si^{28}

(p, 2p, γ) Al^{27}, giving gamma radiation with an energy 0.84 MeV and annihilation γ-quanta.

The $\gamma - \gamma$ background registered by the detectors in sea water consists of cascade radiation of isotopes of natural and artificial origin; the background of cosmic radiation of the cascade type and the processes of registry of a high-energy charged particle by two sensors; random coincidences caused by loading of the spectrometer channel in the detector; characteristic background of the detectors, including errors in the electronic circuits.

As is well known, the counting rate of random coincidences caused by loading of the spectrometer channel of the sensors is expressed by the formula

$$n_{ij} = 2\tau n_{1i} n_{2j}. \quad (13)$$

Here τ is the coincidence circuit resolution time, in our case being 1 ∓ 0.5 m·sec; n_{1j}, n_{2j} are the counting rates (loadings) of sensors with a given discrimination level. We took the data on n_{1j}, n_{2j} in the processing of spectra of total γ-radiation.

The contribution of random coincidences for the real background of γ-radiation in sea water and in the material of the sensors is 10^{-2}–10^{-3} pulses·min^{-1} for the low horizons and 1 pulse·min^{-1} for the surface and is a small part of the intensity of the cascade radiation of sea water. The characteristic $\gamma - \gamma$ background of the detectors, determined under conditions of protection of the sensors by a layer of fresh water, gave values of the same order of magnitude.

The cascade background of cosmic origin is essentially dependent on the measurement horizon. It decreases considerably in the first 10-30 m from the surface and continues to decrease with depth. An examination of the parameters of the γ-background of cosmic origin is the subject of a special investigation. Here it is important to note that it has a considerable spatial anisotropy $I_0 = I_{vert} \cos \alpha\theta$, $\alpha = 2$ for 100 meq, $\alpha = 3$ for 2000 meq. This circumstance makes it possible to discriminate it in the processing of the results of measurements made using different instrument channels.

A fundamental difficulty in measuring the radioactivity of sea water by the direct method is the small level of its activity against the background of considerable fluctuations caused by the nonstationary character of the radiation background in sea water and different kinds of instability of instrument operation. Due to the fact that the inaccuracy in measuring activity is proportional to $\sqrt{N}$, where N is the registered number of gamma quanta, reliable registry of the effect of disturbance of the field of gamma radiation and identification of the factor responsible for this disturbance is possible when there is a sufficiently high statistical probability of measurement, that is, with an increase in the mass of the detector and the measurement time. However, such a means for increasing the statistics is fundamentally limited by the characteristic time scale of

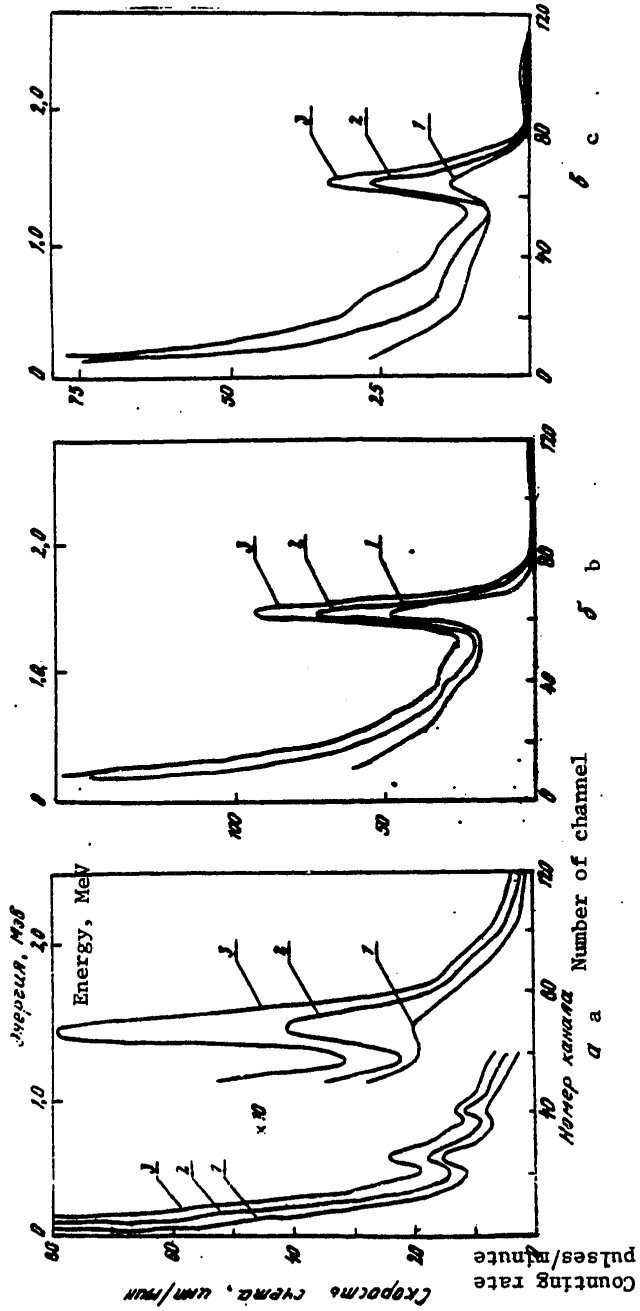

Fig. 5. Spectra of γ-radiation of sea water of different salinity obtained using three detectors (explanations in text).

fluctuation of the radioactivity field, the limited size of the scintillation detectors produced by industry, the uncontrollable instabilities of the spectrometer amplification channel of the instrument and fluctuations of the γ-background of nonradioactive origin.

In this connection the problem arises of the most complete possible use of the information obtained from the radiation detector, that is, the rapid spectrometry of radiation, which in contrast to radiometry makes it possible to identify small-scale fluctuations of radioactivity on the basis of changes in the form of the spectrum during short time intervals. In combination with the multichannel principle, which in itself increases the number of measurable informative criteria of the effect, such changes make it possible to separate fluctuations of nonradioactive origin and apparent disturbances caused by instability of operation of individual measuring apparatus channels. What has been set forth above makes possible a considerable increase in the volume of statistical information for the necessary time intervals and selection of its maximum specifically at the time of maximum field disturbance.

The processing of information must be accomplished using the principle of direct connection between the spectral analyzers and the shipboard computer and includes the following tasks: correction of spectrometric information (channel-by-channel); discrimination of random omissions, failures and "surges," identification and discrimination of background trends and fluctuations caused by the background of cosmic radiation and instability of instrument operation; reduction of channel-by-channel spectrometric information to a single energy scale and accumulation of statistics; discrimination of pulsations of the field of radioactivity of sea water and determination of their spatial-temporal and spectral (energy) parameters; identification of the reasons for fluctuations of the field of radioactivity of sea water on the principle of the generalized least squares method on the basis of information on the spectra of sample sources; determination of the correlations between fluctuations of the field of radioactivity and fluctuations of other hydrological fields and also the correlations of their parameters.

As a result of electric and magnetic induction in the instrument components it is common to observe considerable surges in the spectra; they must be regarded as serious gaps and rejected. The form of such a surge can serve as a criterion for carrying out the operation. They occur during a very short time, considerably less than the exposure time, and therefore an excess of $I^{p}_{\sigma}(E_i)$ over $I^{p}(E_i)$ by a value greater than $3\sigma^{p}(E_i)$ must be assigned to a doubtful case and there must be checking of the nature of the fluctuation with respect to the form of the line in the energy spectrum. If the fluctuations are caused by the appearance of activity in the measured volume, it has the form of a Gauss curve; the presence of a doubtful fluctuation in σ in the energy spectrum can be identified as a surge.

Due to the different kinds of instabilities in operation of the spectrometric channels of the instrument it is virtually impossible to achieve a standard scale for individual channels of the γ-complex; moreover, in the measurement process there can be small long-period fluctuations of the amplification factor for the spectrometers, for example, due to the instability of the temperature regime of the submergible unit, which can lead to apparent temporal fluctuations of activity in the medium. Accordingly, monitoring of the stability of energy calibration of the channels is necessary for correction of time series of spectra, their reduction to a single energy scale in time [10]. Floating calibration of the spectrometers is accomplished on the basis of the reference peaks 1.46, 0.9, 0.55 MeV and 0.5 MeV respectively in the spectra of total and cascade γ-radiation.

The discrimination of fluctuations of intensity of the field of γ-radiation of sea water, instabilities of the instrument and variations of the background of cosmic radiation is accomplished by making an analysis of the mean square values of the relative fluctuations of intensity (R^2) in different channels

$$R^2 > \bar{\theta}_2 - \bar{\theta}_1 - \sqrt{\frac{2}{s}}\,\alpha_s^{(r)}\,(2\varepsilon). \tag{15}$$

Here

$$\bar{\theta}_1 = \frac{\sum (n_\nu - m_\nu - \bar{n} + \bar{m})^2}{\sum (n_\nu + m_\nu)}, \quad \bar{\theta}_2 = \frac{\sum (n_\nu + m_\nu - \bar{n}_\nu - \bar{m}_\nu)^2}{\sum (n_\nu + m_\nu)},$$
$$\nu = 1, 2, \ldots, s,$$

m_ν and n_ν are the intensities in the two analyzed channels; α_s is the reliability criterion; $\sum$ is the significance level.

Incidentally we clarify the relative instability of the instrument channels

$$g = \left(\frac{\theta_1 - 1}{\langle n\rangle + \langle m\rangle}\right)^{1/2}, \tag{16}$$

$\langle n\rangle$, $\langle m\rangle$ are the mathematical expectations of the counting rates in these channels. After obtaining reliable evaluations of the reality of the fluctuations of activity of the sea medium it is possible to combine the time intensity series obtained in different channels for analysis of the spatial-temporal scales of the distribution of activity in the ocean.

Summary

Use of the method of spatial-temporal and energy rejection of the background of interfering radiation on the basis of multichannel spectrometry considerably broadens the possibilities for measuring small activities of the sea medium and increases the reliability of the collected information.

The instrument created on the basis of this principle, operating in a regime of rapid γ-spectrometry, has high informative qualities.

It is desirable that further improvement of the method be carried out on the basis of the multichannel principle with the indispensable condition of processing of the collected information on an electronic computer in real time.

BIBLIOGRAPHY

1. Lavrenchik, V. N., Sofiyev, G. N., "Intensity and Spectral Composition of γ-Radiation of Ocean Water," IZV. AN SSSR, SER. GEOFIZ. (News of the USSR Academy of Sciences, Geophysical Series), No 2, pp 25-27, 1962.

2. Khitrov, L. M., Kotlyarov, K. A., "Deep-Water γ-Radiometer and Measurement of the Radioactivity of Deep Water Layers in the Indian Ocean," OKEANOLOGIYA (Oceanology), 2, pp 16-17, 1962.

3. Vinogradov, A. S., "Optimization of the Submergible Scintillation Sensor Method," MORSKIYE GIDROFIZICHESKIYE ISSLEDOVANIYA (Marine Hydrophysical Investigations), No 3, Sevastopol', pp 191-199, 1969.

4. Vinogradov, A. S., Vinogradova, K. G., "Measurement of the Activity of Sea Water by the Submergible Scintillation Sensor Method," METODIKA I APPARATURA DLYA GIDROFIZICHESKIKH ISSLEDOVANIY (Method and Instrumentation for Hydrophysical Investigations), Kiev, "Nauk. Dumka," pp 122-130, 1969.

5. Batrakov, G. F., et al., "Field of γ-Radiation in the Upper Layer of the Black Sea," ATOMNAYA ENERGIYA (Atomic Energy), Vol 33, No 3, pp 785-788, 1972.

6. Sapozhnikov, Yu. A., et al., "Effectiveness of a Scintillation Detector of γ-Quanta in an Isotropic Emitting Medium," ATOMNAYA ENERGIYA, Vol 40, No 3, pp 246-248, 1976.

7. Pachurova, V. I., TABLITSY INTEGRO-EKSPONENTSIAL'NOY FUNKTSII (Tables of Integrodifferential Functions), Moscow, 1959, 65 pages.

8. Kosourov, G. I., PRIBORY I TEKHNIKA EKSPERIMENTA (Experimental Instruments and Methods), No 5, pp 95-98, 1962.

9. Khayakava, S., FIZIKA KOSMICHESKIKH LUCHEY. CH. I, YADERNO-FIZICHESKIY ASPEKT (Physics of Cosmic Rays. Part I. Nuclear Physics Aspect), Moscow, "Mir," 1973, 96 pages.

10. Vinogradov, A. S., Vinogradova, K. G., "Features in the Processing of Experimental Gamma Spectra in Investigation of Ocean Radioactivity," MORSKIYE GIDROFIZICHESKIYE ISSLEDOVANIYA, No 1, Sevastopol', pp 212-224, 1969.

11. Chesselet, R., "Application en oceanografie de la methode de spectrometrie gamma 'in situ'," REV. INTERNAT. OCEANOGR. MED., pp 5-21, 1967.

12. Chesselet, R., Nordemann, P., "Rapport DE /Sep/ 1563-194," BULL. INT. SCI. TECH., p 64, 1962.

13. Proctor, C. M., "Response of γ-Scintillation Detectors for Field Survey Use," LIMNOLOG. OCEANOGR., 7, pp 273-279, 1962.

14. Riel, C. K., "New Underwater Gamma Spectrometer," ELEKTRONIKA (Electronics), 36, No 10, pp 37-38, 1963.

15. Akijama,T., "On an Instrument for 'in situ' Measurement of γ-Ray Activity in Deep Water of the Ocean," THE OCEANOGRAPHICAL MAGAZINE, Vol 17, No 1-2, 69, 1965.

16. Sybesma, C., "Measurements of Continuous Energy Distribution of Gamma Rays on a Scattering Medium," p 40, Amsterdam, 1961.

[351-5303]

5303
CSO: 1865

TERRESTRIAL GEOPHYSICS

UDC 551.242:551.79(235.211+235.216)

QUATERNARY TECTONICS AND THE ABYSSAL STRUCTURE OF PAMIR AND TYAN'-SHAN'

Moscow SOVETSKAYA GEOLOGIYA in Russian No 2, 1980 pp 78-96

[Article by V. N. Krestnikov, I. L. Nersesov, D. V. Shtange, Earth Physics Institute of the USSR Academy of Sciences]

The study of the abyssal structure of the earth's crust and its relation to the surface tectonic movements remains as before an urgent problem. In one of the first papers on this problem published 18 years ago [5], a quite detailed comparison was made between the nature of development of the earth's crust during the most recent and earlier stages with the M discontinuity relief. Recently new data have been obtained on the Quaternary tectonics of Pamir and Tyan'-Shan' [12], which indicate that the modern structural level was formed basically in a comparatively short time interval — about 1 million years. It is natural that the intensive tectonic movements that have occurred here had an abyssal nature and could not find expression in the M discontinuity relief. For the Quaternary period, predominantly ascending movements and constant buildup of their velocities are characteristic, which distinguishes these movements from the latest, which during the entire period of activation beginning at the end of the Paleogenic, have changed more than once with respect to intensity, and in a number of cases, even with respect to sign. Therefore the investigation of the relation of the M discontinuity relief to the Pleistocene and Holocene movements appears to be more expedient than with the latest as a whole.

History of Quaternary Tectonic Movements and the Modern Structural Level. In Northern and Central Tyan'-Shan', the end of the Pliocene is characterized by attenuation of the tectonic movements and the onset of a quiet period [12]. During this time there were a large number of lakes separated by low gently sloping divides with altitudes to 1000 meters. Somewhat later, in the early Pleistocene, the tectonic movements were attenuated in the rest of the territory of Tyan'-Shan' and in Pamir, where the mountainous country already existed with altitudes at individual points to 3000 meters and more. With the end of the period of tectonic quiet and intensification of tectonic activity begins the Quaternary history of the region itself. The movements of the Quaternary period were attenuated first in the Central and Northern Tyan'-Shan' and somewhat later, in the rest of the territory.

Thus, the Quaternary stage of development began with sharp intensification of differentiated, predominantly ascending movements, the velocities of which successively increased to the Holocene and reached the largest values in the last 10,000 years. During this phase, the modern structural level was formed, the basic features of which were created in the pre-Quaternary time.

On the whole, Tyan'-Shan' and Pamir are a complexly built block mountain structure where both positive and negative structural elements are clearly isolated, which are separated in the majority of cases by dislocations with a break in continuity of various orders. On the diagram of the summary Quaternary vertical movements (Fig 1) it is clearly obvious that in the described region the structural elements of the sublatitudinal Tyan'-Shan' strikes enjoyed a clear advantage, and the anti-Tyan'-Shan' northwesterly and northeasterly direction have subordinate significance.

The territory of Tyan'-Shan' is divided into the western and eastern parts by the Talaso-Fergan abyssal fracture zone of northwesterly strike. During the entire latest stage, especially in the Quaternary period, their development differed significantly.

The eastern part of Tyan'-Shan' which includes Central and Northern Tyan'-Shan' developed as a single block experiencing distortion from south to north during the process of the general uplift. Relatively uniform distribution of uplifts and depressions with respect to area is characteristic of this part. Here a clear trend is noted toward increase in scales of the basins from south to north and scales of the uplifts in the southerly direction. The basic structural elements are elongated in the sublatitudinal direction; in plan view, they are arcs slightly convex to the south. In the north of this part of Tyan'-Shan' there are two large basins -- the Chuyskaya and Iliyskaya -- separated by the uplift of the Kindiktasskiy Mountains, the amplitude of the uplift of which in Quaternary time exceeded 500 meters; the central parts of these depressions experienced absolute downwarping in the Pleistocene.

To the south of the Chuyskaya and Iliyskaya Basins, separated from them by the Northern Tyan'-Shan', Alma-Ata and Zailiyskiy abyssal fracture zones is the system of uplifts of the Kirgizskiy, Zailiyskiy Alatau and Kungey Alatau Ridges. The greatest amplitudes of their Quaternary movement exceed 1000 meters. The uplifts of the Zailiyskiy and Kungey Alatau Ridges are separated by the Kemino-Chilikskiy abyssal fracture zone. The Talasskaya Basin (in the extreme northwest of the territory it connects with the Chuyskaya Basin) is connected to the northeastern end of the KirgizRidge with respect to the Ichkele-Susamyrskiy abyssal fracture. During the Quaternary period, the Talasskaya Basin experienced relative downwarpings.

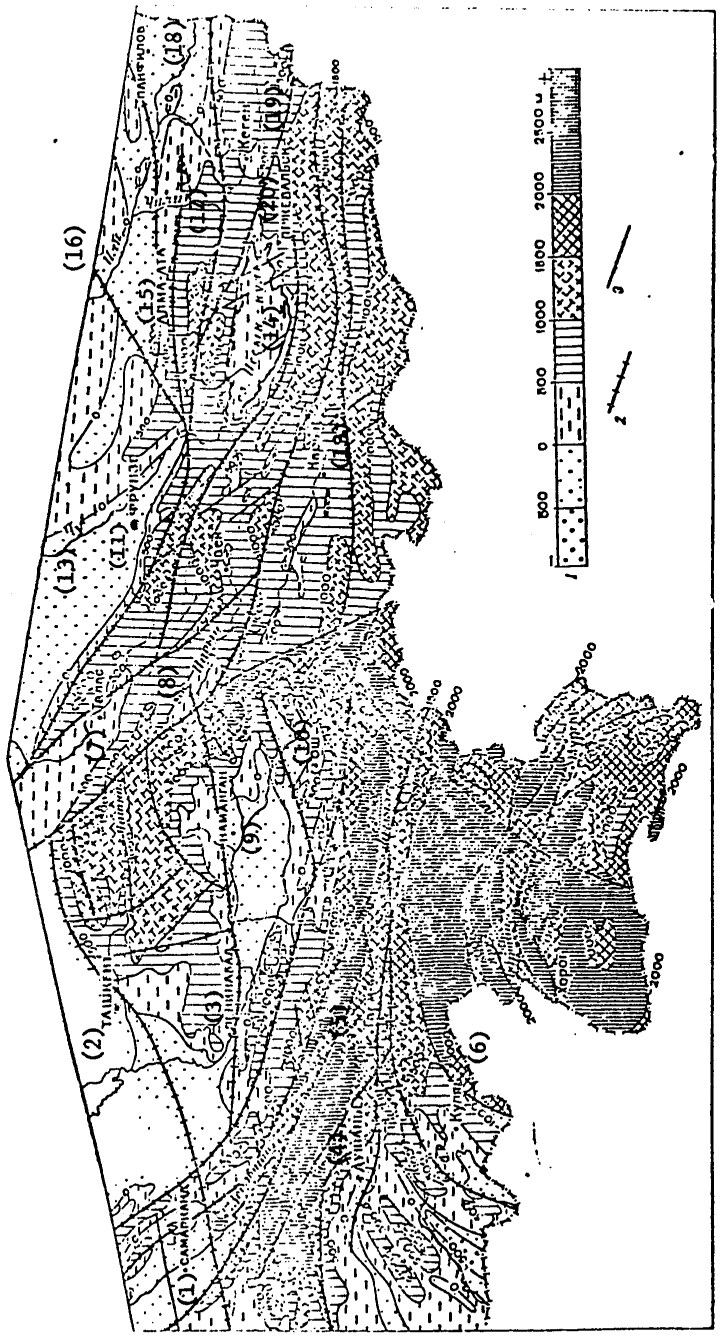

Figure 1. Schematic of the summary vertical tectonic movements in the Quaternary period

1 -- amplitude distribution scale of the vertical tectonic movement; 2 -- abyssal fracture zones; 3 -- regional dislocations with a break in continuity of the anti-Tyan'-Shan' strikes

Key:

1 -- Samarkand; 2 -- Tashkent; 3 -- Leninabad; 4-- Dushanbe; 5 -- Garm; 6 -- Kulyab; 7 -- Talas; 8 -- Naryn; 9 -- Namangan; 10 -- Osh; 11 -- Frunze; 12 -- Chu; 13 -- Kar'n; 14 -- Issyk-kul' Lake; 15 -- Alma-Ata; 16 -- Ili; 17 -- Chilik; 18 -- Panfilov; 19 -- Kegen; 20 -- Przheval'sk

South of the uplift of the Kungey Alatau Ridge is one of the largest basins of Central Tyan'-Shan' -- the Issyk-Kul' Basin, one of the largest basins of the entire region -- where the lacustrine conditions have been maintained to the present time. It is characterized by a relative downwarp in Quaternary time, but it is not excluded that its central part also experienced absolute downwarping. In the northeastern part the Issyk-Kul' Basin is separated from the uplift of the Kungey Alatau Ridge by the Tyupskiy abyssal fracture zone coupled on the west to the Kemino-Chilikskaya zone, and on the east to the Terskey-Talasskaya zone. The Terskey-Talasskiy abyssal fracture zone separates the Issyk-Kul' Basin from the uplift of the Terskey Alatau Ridge, the amplitudes of the movements of which exceed 1000 meters. Together with the uplift of the Kokshaaltau Ridge, it forms one of the largest mountain systems in Central Asia.

Two abyssal fracture zones pass through this system -- the Atbashskaya and the Nikolayev line, with which a number of depression zones are associated. In the west the uplift of the Terskey Alatau Ridge is submerged and becomes the Naryn Basin, relatively downwarped in the Quaternary time. In the south the latter becomes the Atbashskaya Basin coupled with respect to the Atbashskiy abyssal fracture zone with the Atbashskiy Ridge, the amplitude of the ascending movements of which is more than 1000 meters. In the east, the uplift of the Atbashskiy Ridge becomes the Terskey Alatau and Kokshaaltau system. In the western part of Central Tyan'-Shan' the structural elements of the Tyan'-Shan' strike are sharply broken off by the Talaso-Fergan abyssal fracture zone.

The western part of Tyan'-Shan' is characterized by the presence of two large basins absolutely downwarped in Quaternary time and a comparatively small number of smaller ones. An important characteristic of this territory is the clearly expressed trend toward the confluence of individual uplifts into large systems with quite large uplift amplitudes. One of the few independent large positive structural elements -- the Fergan Ridge uplift -- strikes in a northwesterly direction from the Soviet border with China in the southeast to the Naryn River valley in the northwest parallel to the Talaso-Fergan abyssal fracture zone and genetically connected with it [8]. The northeastern limb of the uplift is cut off by a fracture zone, and the southwestern limb smoothly submerges and becomes the Fergan Basin. The maximum uplift amplitudes in the axial part exceed 2000 meters.

The Fergan Basin, which in plan view has a triangular shape, is located to the west of the Fergan Ridge. In the North the Naryno-Chichkanskiy abyssal fracture zone separates it from the uplifts of the Chatkalo-Kuraminskaya Mountain system. In the South along the Southern Fergan abyssal fracture zone it is coupled to the uplift of the Gissaro-Alayskiy Mountain system. The structure of the basin is complex; a number of structural zones and individual structural elements are isolated within its boundaries. In the southeastern part the basin is intersected by the Vuadil'-Kugartskiy abyssal fracture zone. During the Quaternary period, the central part of the basin experienced absolute downwarpings.

The Chatkalo-Kuraminskiy region located north of the Fergan Basin is a system of the latest uplifts and basins of northeasterly strike. Here the Ugamskoye, Sandalashskoye, Chatkalo-Kuraminskoye and Atoynokskoye uplifts are isolated along with the Pskemskiy, Chatkal'skiy, Angrenskiy and Nanayskiy Troughs that separate them. The uplifts and troughs, as a rule, are controlled by dislocations with a break in continuity. In the East, all of the structural elements are broken off by the Talaso-Ferganskiy abyssal fracture zone, and on the Northeast, they are bounded by the Western Tyan'-Shan' abyssal fracture; in the westerly direction the uplifts gradually submerge, becoming complicated by the transverse Chatkalo-Kuraminskiy abyssal fractures. The maximum uplift amplitudes of the Chatkalo-Kuraminskaya Mountain system exceeded 1500 m in the Quaternary period.

The Gissaro-Alayskaya uplift system located south of the Fergan Basin has sublatitudinal Tyan'-Shan' strike, and in the East it is coupled with the Fergan Ridge uplift. The largest structural elements of the system are the uplifts of the Zeravshano-Gissar, the Turkestan and Alay Ridges, the "40th parallel" basin, the Verkhnegul'chinskaya and Pendzhikentskaya Basin and the Zeravshanskiy Trough. With respect to strike the large structural elements are bounded by regional and abyssal fractures.

From the South the Zeravshano-Gissar uplift is controlled by the southern Gissar abyssal fracture zone, and it is separated from the uplift of the Turkestan Ridge parallel to it by the Zeravshanskiy abyssal fracture zone. The Zeravshanskiy Trough located between them traced in the middle and lower courses of the Zeravshan River strikes in a westerly direction to the city of Samarkand.

The uplift of the Turkestan Ridge in the North is separated from the Fergan Basin by the Southern Fergan abyssal fracture zone, along which there is a change of "40th parallel" depressions. From the North the basins are bounded by the system of latitudinally elongated anticlinal uplifts. In the East the uplift of the Turkestan Ridge becomes the Alay uplift, which is also separated from the Fergan Basin by the Southern Fergan abyssal fracture zone, and in the East it is coupled with the uplift of the Fergan Ridge. In the western part of Gissaro-Alay the structural elements undergo virgation and are bounded on the whole by the Western Tyan'-Shan' abyssal fracture zone, to the West of which the amplitudes of the uplifts decrease sharply. Here basically the descending tectonic movements predominated; the maximum amplitudes of the ascending movementa are known in the central part of Gissaro-Alay, where they exceeded 2500 meters in Quaternary time.

The articulation zone of Pamir and Tyan'-Shan' strikes in a sublatitudinal direction, bordering Pamir on the North and on the West. Its southern boundary is the Darvaz-Karakul'skiy abyssal fracture zone; its northern boundary is the Gissaro-Kokshaal'skiy abyssal fracture; in the East is the Alay Basin bordered on the North by the Alay Ridge uplift and on the South by the system of uplifts of Northern Pamir. To the West and South

of the Alay Basin are the uplifts of the Zaalayskiy, Petr Pervyy, Vakhsh, Surkhku and Vneshniy Darvaz Ridges. Southwest of Pamir is the Tadzhik depression, within the boundaries of which several structural zones are isolated. An entire series of uplifts and troughs of predominantly submeridional strike have developed here. The amplitudes of the movements in the Tadzhik depression fluctuate within very broad limits: in the depression zone the absolute downwarpings sometimes exceed 500 meters at the same time as some of the positive structural elements experienced an uplift of more than 1000 meters. The uplift amplitudes of the articulation zone of Pamir and Tyan'-Shan' are maximal in the central and eastern parts (1500 meters) and in the extreme East (2000 meters).

The mountainous structure of Pamir was formed during the process of closure of the Alpine geosynclinal and subsequent ascending differentiated tectonic movements. Its structural elements in plan view form arcs which are convex in the northerly direction. In the formation of the modern structural plan the meridional zonality connected with the development of the Pamiro-Himalayan abyssal fracture zone has great significance [6]. During Quaternary time Pamir was finally separated by this zone into the western and eastern parts which are two large megablocks distinguished with respect to nature of tectonic development.

The largest structural element of Western Pamir is the Northern Pamir uplift located in the vicinity of the Darvazskiy, Vanchskiy, Yazgulemskiy, Academy of Sciences and Northern Tanymas Ridges, the central part of the Zaalayskiy Ridge and the eastern part of Petr Pervyy Ridge. In the North the Darvaz-Karakul'skiy abyssal fracture zone separates it from the Tadzhik depression and Pamiro-Alay; in the South it is bounded by a large regional fracture, and in the East by the Pamiro-Himalayan abyssal fracture zone. The maximum amplitudes of the Quaternary movements of this uplift exceed 2500 meters.

In addition to the Northern Pamir uplift within the boundaries of Western Pamir a number of other, less significant structural elements are isolated: Bartangskiy, Guntskiy, Dzhoushangozskiy and Vakhanskiy Troughs, the western parts of the Rushanskiy and Southern Pamir uplifts. Some latitudinal strikes and good expression in the relief are characteristic of them. The amplitudes of the ascending movements of the Rushanskoye uplift within the boundaries of the Western Pamir zone exceeded 2500 meters, and Southern Pamir, 2000 meters.

In Eastern Pamir the intensity and differentiation of the tectonic movement are appreciably less. In the North the development of the latest structural plan has caused submeridional strikes of the basic structural elements and among them, the largest -- the Karakul'-Kokuybel'skiy Trough, the Akbaytal'skoye and Sarykol'skoye uplifts, the Rangkul'-Aksuyskaya region of relative downwarping. For such large structural elements located in the South as the Vakhanskoye uplift, the Alichurskaya and Zorkul'skaya Basins, the eastern parts of the Rushanskoye and Southern Pamir uplifts,

sublatitudinal strikes are characteristic. All of the positive structural elements of Eastern Pamir experienced ascending movements in the Quaternary time with amplitude exceeding 2000 meters; the basins, just as in Western Pamir experienced relative downwarpings.

On the whole, the investigated region was characterized in Quaternary time but by the predominance of intensive ascending movements, the scale of which was 2000 to 3000 meters or more. The descending movements had subordinate significance and were manifested in local sections. The greatest intensity of movement was reached in Pamir, where their amplitudes within the boundaries of the uplifts exceeded 2000 to 2500 meters everywhere. In Tyan'-Shan' the ascending movements were most intense in the eastern part of the Turkestan Ridge, and their amplitude reached 2500 m.

In the Quaternary period, the differences in tectonic conditions between Western and Eastern Tyan'-Shan' continued to deepen: Western Tyan'-Shan' experienced intensive differentiated movements, and Eastern Tyan'-Shan' developed on the whole as a single block. During this time just as in the pre-Quaternary time, an important role in the tectonics of Pamir and Tyan'-Shan' was played by the abyssal fracture zones. Breaking up the entire earth's crust into blocks, they to a great extent determined the nature of the tectonic development of the territory. Usually these are steeply dipping reverse thrust faults, the amplitudes of the displacement along which vary within broad limits in time and in space. The majority of them are of ancient occurrence, and only the Pamir-Himalayan abyssal fracture zone began to be fixed in the Mesozoic. The strike of the abyssal fractures is predominantly Tyan'-Shan' in accordance with the general structural plan, but some of them have transverse, anti-Tyan'-Shan' strike. The most intensive movements of the Quaternary time occurred along the Darvaz-Karakul', Talaso-Fergan and the Pamir-Himalayan abyssal fracture zones. The least active were the Central Tyan'-Shan' fractures.

In the Quaternary history of Pamir and Tyan'-Shan' obviously the transverse regional dislocations with a break in continuity begin to acquire important significance, which can be combined into two systems: of northwestern and northeastern strikes. For the western part of Tyan'-Shan', the fractures of northeasterly strikes parallel to the Western Tyan'-Shan' abyssal fracture are characteristic, and for the eastern part, northwesterly, parallel to the Talaso-Fergan fracture. The anti-Tyan'-Shan' regional dislocations are fixed well in the structure of the region from the Pleistocene. Part of them are clearly isolated by the geological data, and others, predominantly in Central Tyan'-Shan', are established both by geological and geophysical methods of investigation [4, 11].

The transverse dislocations with a break in continuity attract attention by their high modern tectonic activity. Thus, in the western part of the Tyan'-Shan' (the regions of the Turkestan and the Zeravshanskiy Ridges), all of the terrace complexes are shifted along them. In Central Tyan'-Shan', in particular in the eastern part of the Issyk-Kul' Basin,

they are fixed predominantly by geophysical methods. In addition, according to our observations, the displacements of the planation surface formed at the end of the Pliocene and also the discharges of thermal, radon and sulfuratted water are connected with them. A number of "trenches" are associated with one of the transverse zones at the bottom of the Tyupskiy Bay. These trenches are traced along both of its shores in the form of small bays. The occurrence and the development of anti-Tyan'-Shan' regional fractures in the Quaternary period permits the conclusion that at the present time the previously formed structural plan of Tyan'-Shan' is being rearranged.

The Mohorovičić Discontinuity Relief. The new version of the schematic of the M discontinuity relief is based on seismologic data. The procedure used here was described in detail earlier [5], and it is not considered in this paper. When compiling the new schematic, the data from the results of recording two large industrial blasts -- in the vicinity of Alma-Ata when building the dam at Medeo and in the western part of the region -- were used. The data from recording the blasts at the seismic stations of Central Asia made it possible to obtain more reliable information about the deviations of the times of arrival of the waves at the station from the averaging holograph. Just as before, these deviations were corrected at the expense of hypsometric altitudes of the location of the stations, and the change in travel time of the waves in the sedimentary series.

In addition to the reference blasts, the materials from recording some of the earthquakes in Central Asia and adjacent regions within the limits of the epicentral distances to 800 km were used. When analyzing the results of the observations, the data from the temporary stations of the Complex Seismological Expedition (KSE) of the Earth Physics Institute of the USSR Academy of Sciences which worked on the seismic regionalization of the hydraulic engineering sites of Central Asia were also taken into account. These studies performed from 1963 to 1976 in the Pyandzh, Vakhsh, Ili, Charyn, Chilik river basins and the Naryn River valley significantly expanded our ideas about the nature of the structure of the M discontinuity. In addition, in the Pyandzh River basin, observations were also made in the territory of Afghanistan, which permitted us to obtain a number of determinations of the thickness of the earth's crust also for its northern part. Since the stations of the Complex Seismological Expedition of the Earth Physics Institute of the USSR Academy of Sciences operated primarily in the boundaries of the mountainous part of Central Asia, for estimation of the variation in thicknesses of occurrence of the M discontinuity in adjacent parts of Southern Kazakhstan, published sources were also used [3, 8, 9, 10]. The deep seismic sounding data were gridded with the seismological data in overlapping sections in Northern Tyan'-Shan'. It must be noted that an insignificant number of deep seismic sounding observation points were used for this region (about 15).

When studying the times of deviations from the average hodograph for the entire territory of Central Asia the velocity at the M discontinuity was taken equal to 7.95 to 8.05 km/sec. These velocities obtained by counter blast observation systems do not contradict the previously published data on the value of the boundary velocity and the foot of the crust. The mean wave velocity in the crust considering corrections for the sedimentary series was taken at 6.0-6.1 km/sec. Its values were also checked by earthquakes with different depth of center in Northern Tyan'-Shan', in the Garm region and in the lower course of the Naryn River. The numerous data on the L_g wave propagation in different directions from the earthquake center are additional evidence of the correctness of its estimate. The interference wave obviously quite well characterizes the mean velocity in the earth's crust close to 3.53 km/sec at distances to 800 km. This does not provide grounds for proposing the presence of a significant difference in the mean velocities of the volumetric waves in the crust. The Pg interference wave, which in practice has a velocity of 6.0-6.2 km/sec in all directions also indicates constancy of the mean velocity of the earth's crust.

The new map (Fig 2) differs significantly from the previously published one with high substantiation. Whereas its first version was constructed by approximately 400 values, for the investigated version about 700 were used. The number of observation points in the eastern part of Northern Tyan'-Shan', in the Tadzhik depression, in the northern part of Afghanistan and the northern border of the Fergan Basin was increased significantly.

On the new diagram it is clearly obvious that the predominant strikes of the structural elements of the M discontinuity are sublatitudinal, Tyan'-Shan'. Within the boundaries of Tyan'-Shan' it is possible to isolate two belts of increased thickness of the earth's crust (more than 50 km) separated by a zone of shallow depths of occurrence of the M discontinuity. The individual structural elements of the M discontinuity relief in the majority of cases also have Tyan'-Shan' strike. However, the uplifts and the basins of anti-Tyan'-Shan' strike, for example, in the vicinity of the Talasskaya Basin, the Chatkalo-Kuraminskaya Oblast, the Kindiktasskiy Mountains, and the central part of Issyk-Kul' are noted.

In the M discontinuity relief it is also possible to isolate proposed fracture zones which are established by a sharp increase in horizontal thickness gradients of the earth's crust. Just as the other structural elements, they are primarily Tyan'-Shan' strike, but fractures of anti-Tyan'-Shan', northeasterly and northwesterly strikes are noted among them. In Pamir the pattern of thickness isolines of the earth's crust in general emphasizes the submeridional structural plan. Unfortunately, the data available at the present time permit a schematic of the M discontinuity relief to be compiled for all of Pamir, and they characterize its western part. On the whole, a trend is noted toward an increase in thickness of the earth's crust in the direction from west to east.

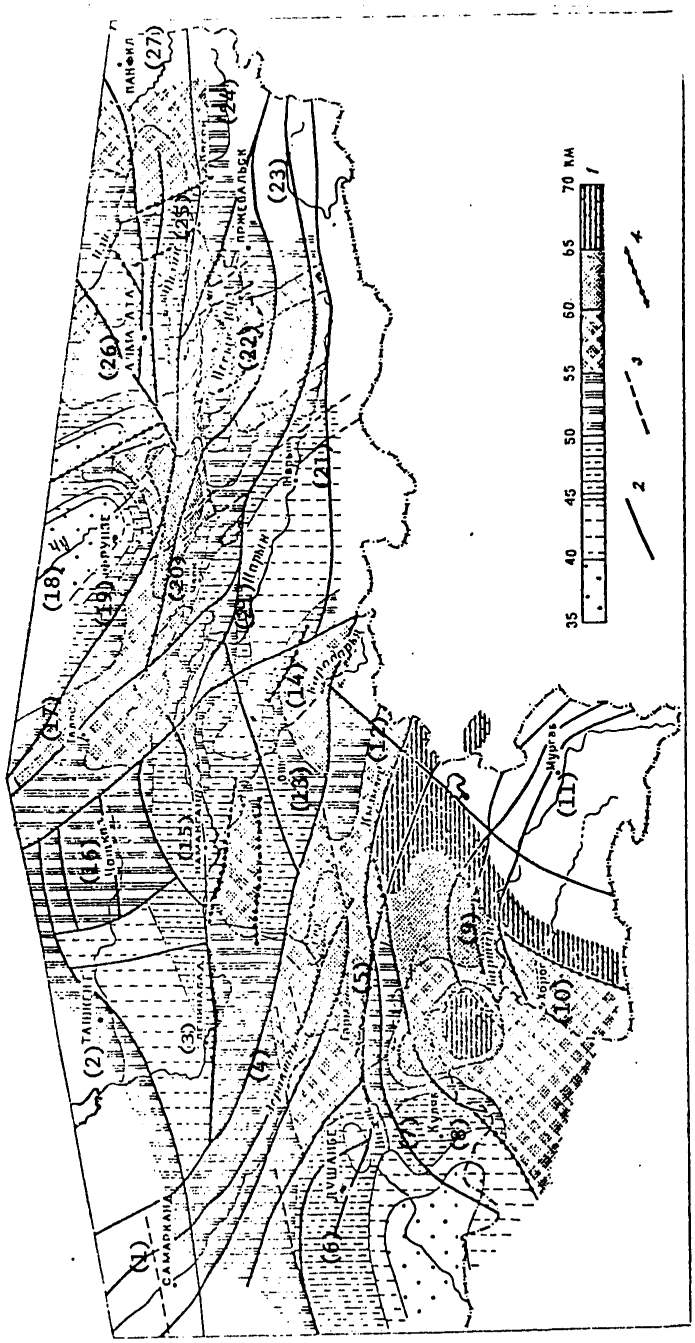

Figure 2. Schematic of the M discontinuity relief
1 -- thickness distribution scale of the earth's crust; 2 -- abyssal fracture zone; 3 -- regional dislocations of the break in continuity of anti-Tyan'-Shan' strike; 4 -- latent dislocations with a break in continuity

Key:
1 -- Samarkand; 2 -- Tashkent; 3 -- Leninabad; 4 -- Zeravtan; 5 -- Garm; 6 -- Dushanbe;
7 -- Vakhsh; 8 -- Kulyab; 9 -- Bartang; 10 -- Khorog; 11 -- Murgab; 12 -- Kyzylets;
13 -- Osh; 14 -- Karadar'ya; 15 -- Namakgan; 16 -- Chatkal; 17 -- Talas; 18 -- Chu;
19 -- Frunze; 20 --Chalk; 21 -- Naryn; 22 -- Issyk-Kul' Lake; 23 -- Przheval'sk;
24 -- Kegen; 25 -- Chilik; 26 -- Alma-Ata; 27 -- Panfilov

Relation of Quaternary Tectonic Movements to the Abyssal Structure. In reference [5] a comparison was made between the ancient and modern tectonics and the M discontinuity relief. Since the new M system does not have theoretical differences from the previously compiled system, it is inexpedient to make such a comparison again. Therefore in this article the M discontinuity relief is considered only in connection with the nature of the Quaternary tectonic movements of Pamir and Tyan'-Shan'. A comparison of the tectonic movements occurring in the last million years with the structure of the earth's crust was made first. With respect to nature of the Quaternary movements within the boundaries of the investigated territory it is possible to isolate three large regions which differ with respect to development and structure -- Eastern Tyan'-Shan', Western Tyan'-Shan' and Pamir. They have also different abyssal structure, but at the same time they have some common features of the M discontinuity relief. Thus, the Tyna'-Shan' strikes of the basic structural elements clearly predominate with subordinate value of the anti-Tyan'-Shan' strikes, and in Pamir the transverse submeridional zonality clearly appears which is characteristic of the latest phase of development of this region. Another current feature is the block structure of the earth's crust of Pamir and Tyan'-Shan'. Here in the overwhelming majority of cases there is a relation between the movement of the blocks of the earth's crust in the Quaternary time and its thickness. The most uplifted blocks correspond also to the greatest depths of occurrence of the M discontinuity, and the subsided ones, the least. However, in a number of cases the inverse relations are also noted. The abyssal fracture zones actively separating the tectonic blocks which developed in Quaternary time in many cases are completely or partially traced in the M discontinuity relief.

The most complex relation between the M discontinuity relief and the vertical Quaternary tectonic movements is noted in the eastern part of Tyan'-Shan', which was developed by a single large block. Within its boundaries positive and negative structural elements of higher orders were formed. From the North along the Northern Tyan'-Shan', Alma-Ata and Zailiyskiy abyssal fracture zones the Chuyskaya and Iliyskaya Basins and also the uplift of the Kindiktasskiy Mountains separating them, which are quite clearly expressed in the M discontinuity relief, are adjacent to this block. The Chuyskaya Basin which on the whole has experienced absolute downwarpings corresponds to reduced thickness of the earth's crust (about 35-40 km), and the uplift of the Kindiktasskiy Mountains, significant thicknesses reaching 60 km in the southeastern part.

The more complex relations of the Quaternary movements and the M discontinuity relief are noted in the Iliyskaya Basin. In its central, most downwarped parts there are regions of both reduced (to 40-45 km) thickness of the earth's crust and increased to 55-60 km. The region of abyssal occurrence of the M discontinuity is in the eastern part of the Iliyskaya Basin and includes the uplift of the Ketmen' Ridge. The system of uplifts of the Kirgiz, Zailiyskiy Alatau and Kungey Alatau Ridges located south of the Chuyskaya and Iliyskaya Basins corresponds to a

significant increase in thickness of the earth's crust -- to 65 km in the central part.

In the vicinity of the Kemino-Chilik Graben, in its Chilik section, the depth of occurrence of the M boundary decreases sharply to 40-50 km. On the east end of the Zailiyskiy and Kungey Alatau Ridges the thickness of the crust also reduces sharply. The presence here and on the west end of the uplift of the Ketmen' Ridge of high thickness gradients of the earth's crust permits the proposition of the existence of latent[1], anti-Tyan'-Shan' dislocations in the break in continuity of northwesterly strike. The latent dislocations of the break in continuity separate a comparatively narrow band of reduced thickness of the earth's crust (45-50 km) of northwesterly strike.

A characteristic structure distinguishes the region of the Issyk-Kul' Basin relatively (and in the central part, possibly, also absolutely) downwarped in Quaternary time. Here the thickness of the earth's crust increases sharply to 60-65 km. In the western part of the basin the depth of occurrence of the M discontinuity also decreases sharply to 45-50 km, and the region of the crust with reduced thickness elongated in the sub-latitudinal direction is also isolated. In the southeasterly direction from the Issyk-Kul' Basin there is a broad strip of increased (to 60-65 km) of the crust traced to the Atbashskiy abyssal fracture zone; south of the latter, there are no data on the depth of occurrence of the M discontinuity. The mentioned strip intersects the system of uplifts of the Terskey Alatau Ridge, which does not find expression in the M discontinuity relief.

It must be noted that the positive structural elements located south of the system of uplifts of the Kirgiz, Zailiyskiy Alatau and the Kungey Alatau Ridges in practice are not expressed in the M discontinuity relief. The small uplifts of the Taktalyk and the Kek-Iyrim-Too Ridges, the amplitudes of the movements of which in the Quaternary time do not exceed 500 meters constitute an exception, but they are well expressed in the M discontinuity relief, the depth of occurrence of which reaches 55-60 km here. At the same time, in the basins of the western part of Central Tyan'-Shan' significant decreases in the thickness of the earth's crust are noted. The Ketmen'tyubinskaya, Susamyrskaya, Chayekskaya and Naryn Basins correspond on the whole to a single uplift in the M discontinuity relief, the depth of occurrence of which is minimal in the Naryn Basin and is 40 to 45 km.. This is the least thickness of the earth's crust known in Central Tyan'-Shan'.

---

[1]By latent, we mean the structural elements well expressed in the M discontinuity relief, but not appearing on the earth's surface.

In the western part of Tyan'-Shan' separated from the eastern zone of the Talaso-Fergan abyssal fracture, in spite of the more complex differentiated Quaternary movement, the M discontinuity relief is somewhat simpler. Even a tectonic suture which is active over the extent of the entire geological history such as the Talaso-Fergan abyssal fracture in practice is not expressed in the M discontinuity relief in the selected cross section. Its structural elements are traced without displacement in both limbs of the fracture. In exactly the same way, the changes in thickness of the earth's crust are also not connected with the uplifts of the Talasskiy and Fergan Ridges next to the fractures [7]. In this part of Tyan'-Shan', just as in the eastern part, significant relations of the Quaternary tectonic movements and the M discontinuity relief are noted.

In the region of the Chatkalo-Kuraminskaya system of uplifts, a comparatively small increase in thickness of the earth's crust to 50-55 km is observed, that is, it has the same value as in the Talas Basin. Thus, the system of uplifts for the maximum amplitudes of the ascending movements in Quaternary time will be more than 1500 meters, and the basin, the amplitude of movements of which does not exceed 500 m, are characterized by identical thicknesses of the earth's crust, and they are not distinguished with respect to the M discontinuity relief. In the direction of plunge of the uplifts of the Chatkalo-Kuraminskiy region the thickness of the crust decreases sharply to 40-45 km along the abyssal fracture zone.

The M discontinuity relief in the Fergan Basin is highly characteristic. In the central section, the thickness of the crust increases sharply to 55-60 km. This region has a shape which is elongated in the sublatitudinal direction; it is bounded from the North and the South by the latent dislocations with a break in continuity. In the western part the crust thickness is somewhat less (50-55 km), that is, the same as in the western part of the Gissaro-Alayskaya system of uplifts. In the extreme eastern part of the basin only the thickness of the crust characteristic for the structural elements -- 40-45 km -- is noted.

A clear relation between the Fergan Basin in the western part of Tyan'-Shan' and the Naryn Basin in the East is detected by the M discontinuity relief. The Gissaro-Alayskaya system of uplifts located south of the Fergan Basin also corresponds to increased thickness of the earth's crust. The intensive tectonic movements of this region, the amplitude of which exceeded 2500 meters in the central zone in the Quaternary time, have found reflection also in the M discontinuity relief. The thickness of its occurrence also reaches 60-65 km here. Both the Tyan'-Shan' and the anti-Tyan'-Shan' directions were reflected in the structure of the M discontinuity. Occupying the central and eastern parts of Gissaro-Alay, the region of increased thicknesses of the earth's crust (55-60 km) is characterized on the whole by sublatitudinal strike, but its western boundary is parallel to the anti-Tyan'-Shan' dislocations with a break in continuity which developed in the Pleistocene and the Holocene, and it is possibly related to them. In the western part of Gissaro-Alay the

Quaternary tectonic movements were less intense, and the thickness of the earth's crust decreases here to 50-55 km, respectively.

For the Tadzhik depression located south of Gissaro-Alay, a significant decrease in thickness of the earth's crust is characteristic. The depression itself experienced relative downwarpings and, in places, even absolute downwarpings in Quaternary time. In the M discontinuity relief it corresponds to the uplift, the central part of which coincides with the most intensely downwarped region of the Tadzhik depression. The depth of its occurrence will be 35-40 km here. In the articulation zone of Pamir and Tyan'-Shan', a decrease in thickness of the earth's crust to 50-55 km is observed. This is much less than in the adjacent regions of Pamir and Gissaro-Alay. In the eastern part of the articulation zone (the vicinity of the Alayskaya Basin) this reduction in thickness of the earth's crust is not noted.

In Western Pamir where the intensity of the ascending Quaternary movements is very great, the depth of occurrence of the M discontinuity increases sharply. However, no clear relation of the surface structure of the plan to the thickness of the earth's crust is noted. Only such large structural elements as the Northern Pamir uplift, the amplitude of uplift of which exceeded 2500 meters in Quaternary time finds some reflection in the M discontinuity relief. This uplift is connected with an increase in depth of its occurrence to 60-65 km and also an increase in the dimensions of the region of great thicknesses of the crust. On the whole, the M discontinuity relief in the territory of Western Pamir has submeridional zonality expressed in the fact that from West to East the thickness of the earth's crust increases, and in the vicinity of the Pamiro-Himalayan abyssal fracture zone it reaches 65 km or more. Unfortunately, the data on the M discontinuity in Eastern Pamir is unavailable; therefore it does not appear possible to talk about general laws for all of Pamir.

A comparison of the surface structure of the plan formed in the Quaternary period with the structural plan of the M discontinuity will permit isolation of large tectonic blocks which have developed in the entire volume of the earth's crust in the investigated region.

In the eastern part of Tyan'-Shan' in the North is the Chu-Iliyskiy block which belongs to the slightly activated part of the epipaleozoic platform. On the South it is bounded by the Northern Tyan'-Shan', Alma-Ata and the Zailiyskiy abyssal fracture zones. For this block, in spite of its significant differentiation, the descending Quaternary movements and comparatively shallow depths of occurrence of the M discontinuity are characteristic in general.

South of Chu-Iliyskiy, the Northern Tyan'-Shan' block is isolated, within the boundaries of which there are a number of large uplifts and basins. On the whole, in Quaternary time it experienced intensive uplift, and the thickness of the earth's crust reaches significant values here.

Southwest of Northern Tyan'-Shan' is the Naryno-Fergan block -- the most complex with respect to structure. Such large basins of Tyan'-Shan' as Naryn and Fergan and also the uplifts of the Chatkalo-Kuraminskaya Mountain system are isolated here. With respect to nature of the M discontinuity relief, the regions located on both sides of the Talaso-Fergan abyssal fracture belong to this block, but the data on the structure of the M discontinuity indicate that at least at the present time this fracture does not play a significant role in the abyssal structure of the earth's crust. Within the boundaries of the Naryn-Fergan block the thickness of the crust varies within quite broad limits -- from 49-50 to 55-60 km, but on the whole the occurrence of the M discontinuity is predominantly shallow here.

The Gissaro-Alayskiy block located to the South and separated from the Naryno-Fergan block by the Southern Fergan abyssal fracture zone is characterized by great thicknesses of the earth's crust. At the same time the intensity of the latest and the Quaternary movements here was significant. Thus, in this block the relation of the surface deformations of the earth and the M discontinuity is normal, just as in the other, Tadzhik block, the surface structure of which corresponds to the Tadzhik depression. Here the regions of relative downwarping, and in places, even absolute downwarping, correspond to a sharp decrease in thickness of the earth's crust. The most downwarped part of the depression also corresponds to the minimum depth of occurrence of the M discontinuity.

To the East of the Tadzhik block, separated from it and from the Gissaro-Alay block by the Darvaz-Karakul'skiy abyssal fracture zone is the tectonic block of Western Pamir. This block, which in this part of Asia experienced the most intense Quaternary ascending tectonic movements is characterized also by the greatest thicknesses of the earth's crust. It is entirely possible that further studies of Pamir will permit estimation of the structure of the M discontinuity even in its eastern part. It is possible to expect that it will be isolated as an independent tectonic block inasmuch as the nature of its development in the modern and specially Quaternary time differ sharply from that in the western part of Pamir, and it differs from the latter by the largest abyssal fracture zone in Asia, the Pamiro-Himalayan.

Thus, by the data from studying the Quaternary tectonic and the structure of the M discontinuity within the boundaries of Tyan'-Shan' and Pamir it is possible to isolate six large blocks of the earth's crust distinguished by geological structure and development: the various relations between the direction and intensity of the Quaternary tectonic movements, the thickness of the earth's crust, and so on. However, they are also characterized by a general law -- the more intense and stable the Quaternary ascending movements, the greater the depths of occurrence of the M discontinuity corresponding to them, and vice versa.

In recent years, with the development of the procedure of seismologic investigation, studies have been made of the horizontal nonuniformities

of the upper mantle. In Tyan'-Shan' and Pamir the given problem has been the subject of papers by L. P. Vinnik and A. A. Lukk [1, 2]. The authors of these papers compiled schematics of the lateral variations of the propagation rate of the longitudinal wave in the upper mantle and they made an effort to compare them with the latest tectonic movement and the relief of this part of Asia. Such systems with some generalizations and additions in Pamir made by the authors of the given article are presented in Fig 3.

It was noted above that the relations of the surface structure of the earth's crust and the M discontinuity relief in Tyan'-Shan' and Pamir are complex and varied. In a number of cases, the structural element of the earth's surface and the foot of the crust do not have mutual correspondence or expression. Therefore direct comparison of the latest tectonic movements and horizontal nonuniformities of the upper mantle is highly possible without considering the structure of the intermediate layer -- the deep horizons of the earth's crust. Unfortunately, the data on the variations of the mean propagation rate of the longitudinal waves in the upper mantle only exist for part of the described territory, which does not permit discovery of the general relations between the horizontal nonuniformities of the upper mantle, the structure and the latest development of the earth's crust for the entire region. However, a comparison of even these available materials is of significant interest.

In Central and Northern Tyan'-Shan' in the upper 150 km of mantle, depending on the nature of propagation of the longitudinal waves, regions of high, low and intermediate velocities are isolated (see Fig 3). A comparison of them with the latest structural plan has demonstrated the following [1]. The regions of high velocities in the plan coincide with the largest depressions of this part of Tyan'-Shan': Iliyskaya and Issykkul'skaya. The low velocity regions extend toward the intensely developed uplifts of the Kungey Alatau, Zailiyskiy Alatau, Terskey Alatau, Kokshaaltau and Kirgiz Ridges, and the intermediate longitudinal wave velocities are noted both in the vicinities of the depressions and the uplifts. However, this is not a general law. In the large depressions -- Chuyskaya and Naryn -- intermediate and not high longitudinal wave velocities are characteristic for the upper mantle; the same velocities are also characteristic of the regions of such large uplifts as the Atbashskiy Ridge, the western end of the Terskey Alatau Ridge, the system of uplifts of the Dzhumgal-Too Ridge, and so on. In addition, the regions of high velocity do not wholly encompass the Iliyskaya and the Issykkul'skaya Basins,but only parts of them; the regions of low velocities, in exactly the same way do not completely correspond to the uplifts with which they are associated.

More defined laws appear when comparing the horizontal nonuniformities of the upper mantle with the structural plan formed as a result of the Quaternary vertical tectonic movements and with the M discontinuity relief. Here it turns out that the regions of high velocities explictly extend to the sections of the large basins in which the increased thickness of the

earth's crust is noted, for example, the western and eastern parts of the Iliyskaya Basin and the eastern part of Issyk-Kul'. The regions of low velocities of the longitudinal waves are also connected with an increase in thickness of the earth's crust, but in combination with the intense ascending tectonic movements, especially the end of the Quaternary period. In cases where the depressions or parts of them correspond to a decrease in thickness of the crust (for example, the Naryn, the Chuyskaya, the central part of the Iliyskaya, western part of Issyk-Kul'), in the regions of the upper mantle corresponding to them, intermediate longitudinal wave velocities are observed. The same values of the longitudinal wave velocities are fixed in the regions of the uplifts in the case where reduced thicknesses of the earth's crust correspond to them, as is noted for a number of intensely developing positive structural elements which we have discussed earlier.

If the discovered law is weak for all of Tyan'-Shan', then on the general level it is possible to expect that the central part of the Fergan Basin will correspond to the region of high longitudinal wave velocities; the Tadzhik depression will correspond to intermediate; the central and eastern parts of Gissaro-Alay will correspond to low. It is necessary to note that in Central and Northern Tyan'-Shan' the transverse anti-Tyan'-Shan' directions are expressed in the horizontal nonuniformities of the upper mantle much worse than in the M discontinuity relief.

In the vicinity of the Alpine geosynclinal, in Pamir, the average propagation rates of the longitudinal waves in the upper mantle is approximately 2 to 3% higher than in Tyan'-Shan', which undoubtedly is connected with the peculiarities of the development of this region. However, just as in Tyan'-Shan', it is possible to isolate regions of relatively high, low and intermediate longitudinal wave velocities (Fig 3). For clarity and convenience of comparison these three qualitative relations both in Pamir and in Tyan'-Shan' are indicated in unique provisional notation independent of the absolute magnitudes of the velocities. This is also caused by the fact that when discovering the general laws of the geologically heterogeneous territories it is more expedient to use the relative characteristics permitting estimation not only of the differences, but also similarity.

In Pamir, in contrast to Tyan'-Shan' between the surface structure of the earth's crust, the M discontinuity relief and the horizontal nonuniformities of the upper mantle no relation is observed. Probably this arises from the rearrangement of the structural level of the described region taking place in the latest, especially in Quaternary time, in which the predominant role began to be played by meridional directions. Thus, the Pamiro-Himalayan abyssal fracture zone which developed actively in the earth's crust and penetrates deeply into the mantle, cuts the focal region of the Pamir-Gindukushskiy deep earthquakes, separating it into two parts -- Murgabskaya and Khorogskaya [6]. Obviously the separation of the regions of intermediate longitudinal wave velocities in the upper mantle

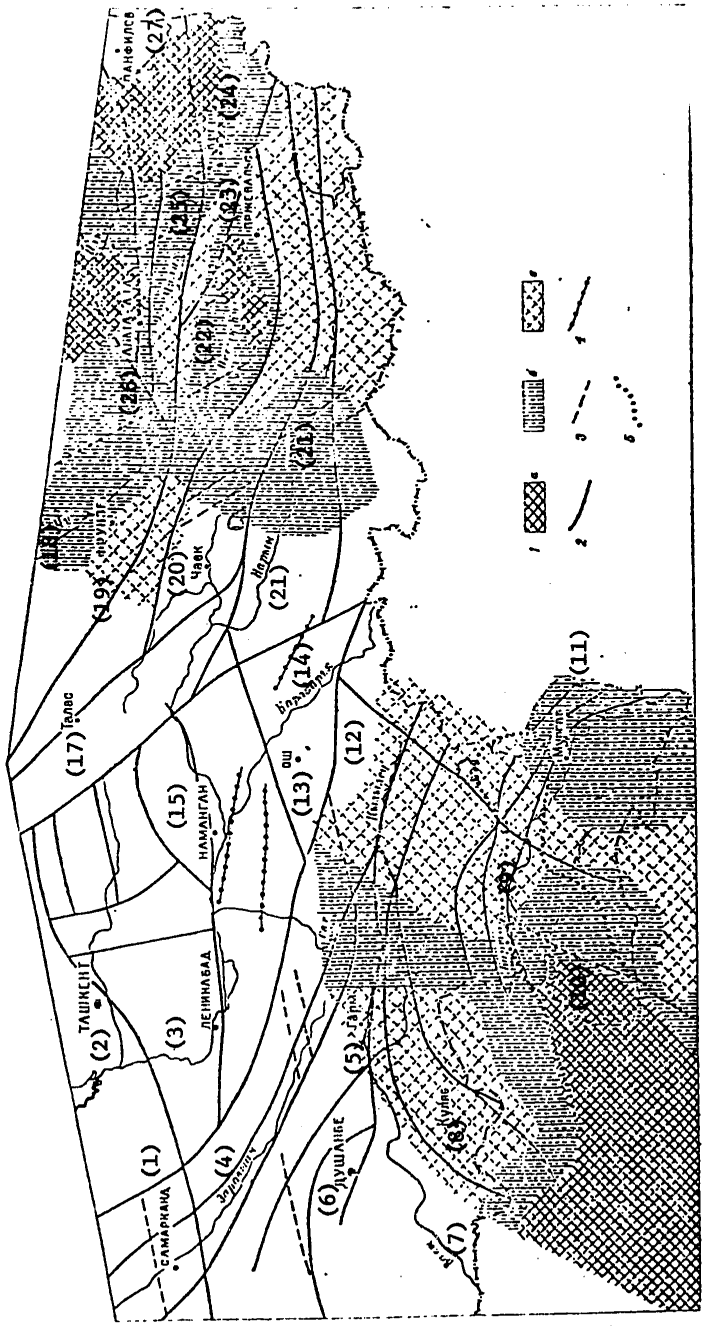

Figure 3. Schematic of versions of the average longitudinal wave propagation velocity in the upper mantle of the Central and Northern Tyan'-Shan' and Pamir.
1 -- mean propagation rate of longitudinal waves (according to L. P. Vinnik and A. A. Lukk with supplements by the authors on Pamir): a -- high (v_p>8.15 km/sec in Tyan'-Shan', v_p>8.36 km/sec in Pamir), b -- intermediate (7.85<v_p<8.15 km/sec in Tyan'-Shan'; 8.2<v_p<8.36 km/sec in Pamir); c -- low (v_p<7.85 km/sec in Tyan'-Shan'; v_p<8.2 km/sec in Pamir); 2 -- abyssal fracture zone; 3 -- regional dislocations with break in continuity of anti-Tyan'-Shan' strikes; 4 -- latent dislocations with a break in continuity; 5 -- epicentral zone of the deep-focus Pamir-Gindukushskiy earthquakes. [See key to Fig 2].

is connected with it. This again confirms the abyssal nature of the rearrangement of the structural level occurring in Pamir in latest time and the significance of the Pamiro-Himalayan fracture zone in the development not only of the earth's crust, but also significantly deeper horizons. In addition, the general location of the regions with different longitudinal wave velocities in the upper mantle, their form in plan, the outlines of the boundaries also confirm the proposition of the existence in the mantle of meridional zonality to depths of 200-250 km.

In spite of the sharp differences in development, Pamir and Tyan'-Shan' have a common important feature: the abyssal fracture zones (with the exception of the Pamir-Himalayan zone) which are quite clearly expressed in the M discontinuity relief are not isolated in the upper mantle according to the data on the variations of the longitudinal wave velocities. Penetrating into the mantle, they clearly damp, not reaching depths of 150 to 250 km for which the determinations of the longitudinal wave velocities were made.

Thus, the analysis of a new schematic of the M discontinuity relief and comparison of it with the modern structural level and the Quaternary tectonic movements as a whole confirm the basic conclusions drawn by the authors earlier [5]. The appearance of a large number of new seismologic data permitted highly reliable estimation of the peculiarities of the abyssal structure of Pamir and Tyan'-Shan'. In particular, they confirm the block structure of the earth's crust of this region. The large tectonic blocks are bounded by the vertical and subvertical abyssal fracture zones penetrating into the mantle and completely or partially expressed in the M discontinuity relief. By the geological data, the abyssal fractures in the majority of cases have developed since the beginning of the Paleozoic or even since the Pre-Cambrian. This permits the proposition that the separation of the earth's crust of the described region into a number of large bounded blocks began in the Phanerozoic. The existence of horizontal submeridional compression during the period of formation of the blocks obviously determined their linear sublatitudinal elongation. Each of the tectonic blocks is complicated by a large structural complex consolidated at a different time.

The studies of recent years have made it possible quantitatively to estimate the intensity of the tectonic movement of Pamir and Tyan'-Shan' in Quaternary time. A comparison of them with the M discontinuity relief offered the possibility of discovering the basic laws of development of the earth's crust in its entire volume in the last million years. The tectonic development of this region in the Pleistocene and the Holocene occurred on the whole inherited; the structural plan did not change significantly by comparison with the Neogenic part of the activation stage. The performed comparison confirmed the existence of a defined relation between the nature of the movements of the isolated blocks of the earth's crust and the M discontinuity relief. The blocks with high intensity of the ascending movements also correspond to great thicknesses of the earth's crust, and vice versa, the thinnest crust characterizes

the block expressing the predominantly descending movements. However, the effectiveness of the Quaternary movements, just as the latest on the whole is connected with the consolidation time. The blocks consolidated in the early stages are characterized by less intense movements and, as a rule, they have a thinner crust.

Thus, the thickness of the earth's crust and the nature of the tectonic movements in the general case can indicate the consolidation time of one block or another. At the same time the interrelations of the tectonic movements and the M discontinuity relief are very complex and varied: the increase in thickness of the earth's crust does not correspond to any uplift on the surface, and the decrease does not correspond to any depression. The most clearly inverse relation (the uplift is the thin crust, the depression, thick) is expressed in the central parts of the Fergan, Iliyskaya and Issyk-Kul' Basins where the depth of occurrence of the M discontinuity increases sharply and also in the Chatkalo-Kuraminskaya Mountain system of uplifts where the thickness of the earth's crust decreases significantly. The uplifts of the Fergan and the Talas Ridges actively developing in the latest and Quaternary time in general are not expressed in the M discontinuity relief.

It is known that during the entire Mesozoic and the greater part of the Paleogene in Tyan'-Shan', the platform conditions existed, and the territory of Pamir and Tyan'-Shan' was leveled. At that time the earth's crust was in a state of isostatic equilibrium and, what is characteristic of the platforms, should have had comparatively small and sustained thickness. Consequently, the modern M discontinuity relief was formed as a result of the endogenic activation beginning at the end of the Paleogenic and subsequent intense tectonic movements of the Neogenic-Quaternary time. It appears that there is a continuous relation between the processes causing deformation of the M discontinuity and the tectonic movements expressed in the surface structure. If this is so, it is possible to state that the deformation of the M discontinuity occurred not continuously, but just as in modern times, there were periods of quiet or deformations of inverse signs even occurred. The latter phenomenon probably is characteristic of the eastern part of Tyan'-Shan' where at the end of the Pliocene, the ascending movements were replaced by descending movements, and with the beginning of the Pleistocene, the ascending movements again sharply predominated.

Thus, the M discontinuity relief was formed obviously basically in a comparatively short time -- during the Quaternary period, that is, it is possible to talk about variation in structure of the entire earth's crust in geological respects in this part of Asia. An important characteristic feature of the Quaternary history of the investigated territory is the development of anti-Tyan'-Shan' structural elements. In the surface structure they began to be fixed only in the beginning of the Pleistocene, but are clearly isolated in the M discontinuity relief. At the same time

there are structural elements, in particular, the Talaso-Fergan abyssal fracture zone which actively developed during the entire activation phase, but nevertheless were not expressed in the M discontinuity relief. In addition, the existence of latent dislocations of the break in continuity and other structural elements not manifested in the surface structure is noted.

All of this permits the proposition that in Quaternary time the process of rearrangement of the structural plan of the earth's crust of Pamir and Tyan'-Shan' takes place. Here an important role begins to be played by the transverse anti-Tyan'-Shan' directions. Inasmuch as the rates of the ascending movements constantly increase from early Pleistocene to the Holocene, it is possible to assume that the intensity of the arrangement also increases. It is entirely possible that the occurrence of the relations for which the uplifts correspond to small thicknesses of the earth's crust and the basins, large ones, is also connected with rearrangement.

A comparison of the latest structural plan, the M discontinuity relief and the horizontal nonuniformities of the upper mantle has demonstrated the following. In Northern and Central Tyan'-Shan' the lateral variations of the longitudinal wave propagation rates in the upper mantle are caused by the structure of the earth's crust as a whole, determining the sub-latitudinal Tyan'-Shan' directions with weakly expressed anti-Tyan'-Shan'. In Pamir the picture is somewhat different. The horizontal nonuniformities of the mantle at depths of 200-250 km confirm the submeridional directions here which are characteristic of the rearrangement taking place and clearly manifested in the M discontinuity relief; in the surface structure of the earth's crust they are almost not expressed. The difference in abyssal structure of these two regions can be caused both by the fact that in Pamir the rearrangement takes place more intensely than in Tyan'-Shan' and by the fact that it began there earlier, possibly in the Paleogenic with general endogenic activation of the tectonic movements or even at the end of the Mesozoic.

Thus, it is possible to draw the conclusion that the generation of large structural forms of the earth's crust in this part of Asia is taking place in the upper mantle at depths of no less than 200-250 km.

BIBLIOGRAPHY

1. Vinnik, L. P.; Lukk, A. A. "Horizontal Nonuniformities of the Upper Mantle in the Regions of Platform Activation of Central Asia," IZV. AN SSSR. FIZIKA ZEMLI [News of the USSR Academy of Sciences. Earth Physics], No 7, 1975, pp 15-29.

2. Vinnik, L. P.; Lukk, A. A.; Mirzokurbanov, M.. "Quantitative Analysis of the Velocity Nonuniformities of the Upper Mantle of Pamiro-Gindukush," IZV. AN SSSR. FIZIKA ZEMLI, No 5, 1978, pp 3-15.

3. ZEMNAYA KORA I VERKHIYAYA MANTIYA SREDNEY AZII [Earth's Crust and Upper Mantle of Central Asia], edited by I. Kh. Khamrabayev, Moscow, Nauka, 1977.

4. Knauf, V. I. "Abyssal-Block Nature of the Structure of Tyan'-Shan'," TRUDY UPRAVLENIYA GEOLOGII I OKHRANY NEDR PRI SM KIRGSSR [Works of the Administration of Geology and Conservation of Minerals under the Council of Ministers of the Kirgiz SSR], No 2, 1962.

5. Krestnikov, V. N.; Nersesov, I. L. "Tectonic Structure of Pamir and Tyan'-Shan' and Its Relation to the Mohorovičić Discontinuity Relief," SOV. GEOLOGIYA [Soviet Geology], No 11, 1962, pp 36-69.

6. Krestnikov, V. N.; Shtange, D. V. "Pamir-Himalayan Abyssal Fracture Zone," IZV. AN SSSR. FIZIKA ZEMLI, No 7, 1977, pp 16-26.

7. Krestnikov, V. N.; Shtange, D. V. "Quaternary History and Seismicity of the Talas-Fergan Abyssal Fracture Zone," IZV. AN SSSR. FIZIKA ZEMLI, No 6, 1979, pp 31-46.

8. Kunin, N. Ya.; Ivanov, A. P.; Shatsilov, V. I. "Abyssal Structure of the Earth's Crust," GEOLOGIYA SSSR [Geology of the USSR], Vol 40, Moscow, Nedra, 1971.

9. Kunin, N. Ya.; Shatsilov, V. I.; Ivanov, A. P. "Abyssal Structure of Southern Kazakhstan According to the Results of Deep Seismic Sounding," BYUL. MOIP. OTD. GEOL. [Moscow Society of Naturalists Bulletin, Geology Division], No 6, 1970, pp 53-66.

10. Pushkarev, I. K.; Ivanov, A. P.; Shatsilov, V. I. "Abyssal Seismic Studies by the Arys'-Balkhash Profile," GEOFIZICHESKIYE ISSLEDOVANIYA V KAZAKHSTANE [Geophysical Studies in Kazakhstan], Alma-Ata, 1968, pp 43-47.

11. Rezvoy, D. P. "Anti-Tyan'-Shan' Structural Direction of the Tectonics of Central Asia," GEOL. SB. L'VOVSKOGO GEOL. O-VA [Geological Collection of the L'vov Geological Society], No 9, Moscow, Nedra, 1965.

12. Krestnikov, V. N.; Belousov, T. P.; Yermilin, V. I., et al. CHETVERTICHNAYA TEKTONIKA PAMIRA I TYAN'-SHANya [Quaternary Tectonics of Pamir and Tyan'-Shan'], Moscow, Nauka, 1979.

[8144/1433-10845]

10845
CSO: 8144/1433

-END-

APPROVED FOR RELEASE: 2007/02/08: CIA-RDP82-00850R000300020046-6